Title: **MSK phosphorylation of H3S28 is required for immediate early gene induction and cardiac hypertrophy**

Running title: **MSK-mediates cardiac hypertrophy**

Emma L. Robinson[1,2*†], Faye M Drawnel[3,4*], Saher Mehdi[1*], Caroline R. Archer[3], Wei Liu[5], Hanneke Okkenhaug[3], Kanar Alkass[6], Jan Magnus Aronsen[7,8], Chandan K Nagaraju[1], Ivar Sjaastad[7,9], Karin R Sipido[1], Olaf Bergmann[10], J. Simon C. Arthur[11], Xin Wang[5], and H. Llewelyn Roderick[1,9†]

[1] KU Leuven, Department of Cardiovascular Sciences, Laboratory of Experimental Cardiology, B-3000, Leuven, Belgium.

[2] Department of Cardiology, Cardiovascular Research Institute Maastricht, Maastricht University, The Netherlands

[3] Epigenetics and Signalling Programmes, Babraham Institute, Cambridge, United Kingdom

[4] Roche Pharma Research and Early Development, Roche Innovation Center Basel, F. Hoffmann-La Roche Ltd, Basel, Switzerland

[5] Faculty of Biology, Medicine and Health, University of Manchester, United Kingdom

[6] Karolinska Institutet, BioClinicum, Oncology and Pathology, SE-17177 Stockholm, Sweden; The National Board of Forensic Medicine, Stockholm, Sweden

[7] Institute for Experimental Medical Research, Oslo University Hospital and University of Oslo, Oslo, Norway

[8] Bjørknes College, Oslo, Norway

[9] KG Jebsen Center for Cardiac Research, University of Oslo, Norway

[10] Karolinska Institutet, Biomedicum, Cell and Molecular Biology, SE-17177 Stockholm, Sweden

[11] Division of Immunology and Cell Signalling, School of Life Sciences, University of Dundee, Dundee, United Kingdom

*These authors contributed equally

†For correspondence: *E-mail:* llewelyn.roderick@kuleuven.be; e.robinson@maastrichtuniversity.nl

Some of this work was carried out while ELR and HLR were at the Babraham Institute.

Current affiliations: CA is at Safety and ADME Translational Sciences, Drug Safety and Metabolism, IMED Biotech Unit, AstraZeneca, Cambridge, United Kingdom. SM is at Wellowise, Research and Development, IIIT Innovation and Incubation, IIIT Delhi, New Delhi, India. HO is at the Imaging Facility, Babraham Institute, Cambridge, United Kingdom

Key words: cardiomyocyte; MSK; phosphorylated Histone 3 Serine 28; immediate early genes; hypertrophy

Brief summary one sentence: MSK1/2 phosphorylation of Histone 3 Serine 28 couples MAPK signalling with chromatin remodelling and immediate early gene expression to induce pro-hypertrophic cardiac transcriptional responses.

Abbreviations:

Ascending aortic banding, AB; atrial natriuretic factor, ANF/Nppa; brain natriuretic factor; BNP/Nppb; cardiovascular disease, CVD; chromatin immunoprecipitation, ChIP; cytosine b-D-arabinofuranoside; ara-C; Ca^{2+}/calmodulin-dependent protein kinase, CaMKII; endothelin-1, ET-1; extracellular signal-regulated kinase 1/2, ERK1/2; fractional shortening, FS; G-protein coupled receptor, GPCR; heart failure, HF; Histone 3, H3; Histone H3 Serine 10, H3S10; phosphorylated H3S10, p-H3S10; Histone H3 Serine 28, H3S28; phosphorylated H3S28, pH3S28, hours, h; immediate early gene, IEG; knockout, KO; mitogen activated protein kinase, MAPK; mitogen and stress activated kinase, MSK; isoproterenol, Iso; minutes, min; myosin heavy chain, α isoform, α-MHC; myosin heavy chain, β isoform, β-MHC; neonatal rat ventricular myocytes, NRVMs; nuclear factor of activated T cells, NFAT; PD184352 (inhibitor of the upstream kinase of ERK1/2, MEK1/2), PD; posterior wall thickness in diastole, PWd; serum response factor, SRF; transverse aortic constriction, TAC; small interfering RNA, siRNA; wild type, WT.

Abstract

Heart failure is a leading cause of death, developing subsequent to deleterious hypertrophic cardiac remodelling associated with pathologies including hypertension and myocardial infarction. MAPK signalling pathways, acting via transcription factors, play a key role in coordinating the induction of gene expression during hypertrophy. Induction of the immediate early gene (IEG) response, characterised by increased expression of AP-1 factors, is a necessary and early event in this process. How MAPK signalling and IEG expression are coupled during cardiac hypertrophy is not yet resolved. Here, in vitro, in rodent models and in human samples, we demonstrate that the MAPK-stimulated IEG response depends on the mitogen and stress activated protein kinase (MSK) and its phosphorylation of histone H3 at serine 28 (H3S28). Brg-1, a BAF60 ATP-dependent chromatin remodelling complex component, is recruited to IEG promoters harbouring phosphorylated H3S28, initiating their expression. In the absence of MSK activity and IEG induction, the hypertrophic response is suppressed. Together, these studies provide new mechanistic insights into hypertrophic gene regulation and highlight the role of signalling to the epigenome in cardiac hypertrophy.

Introduction

Cardiovascular diseases (CVDs) are the leading cause of mortality and morbidity worldwide (Savarese and Lund, 2017). While cardiac hypertrophy is initially an adaptive response to increased workload or stress that enables cardiac function to meet the changing needs of the organism, when induced by pathological cues such as aortic stenosis, prolonged hypertension or myocardial infarction, over time, the response can decompensate resulting in a decline in cardiac function and progression to heart failure. At the cellular level, owing to their terminally differentiated status, hypertrophy of the cardiac muscle is mediated by growth of existing cardiomyocytes and not through their proliferation (Alkass et al., 2015).

Signalling pathways activated downstream of G protein coupled receptors (GPCR), such as those liganded by endothelin-1 (ET-1) and angiotensin II play a fundamental role in the induction of pathological hypertrophic remodelling. Owing to their nodal position in pathways downstream of GPCR activation, Mitogen Activated Protein Kinases (MAPK) are of particular importance in induction of hypertrophic growth of cardiomyocytes (Auger-Messier et al., 2013; Liao et al., 2001). Indeed, MAPK signalling pathways affect pathological hypertrophic growth via regulation of protein synthesis, metabolism and gene transcription.

MAPKs fall into three major families which are categorised according to the terminal kinase in the pathway – the extracellular regulated kinases 1 and 2 (ERK1/2), p38 MAPK and c-Jun N-terminal kinases 1 and two (JNK1/2) (Bueno et al., 2000). Involvement of all three limbs of this family of kinases has been demonstrated in regulating hypertrophic remodelling, the phenotypic outcome differs depending upon the relative activation of each family member (Garrington and Johnson, 1999; Heineke and Molkentin, 2006). For example, enhanced ERK signalling leads to concentric

cardiac hypertrophy with preserved cardiac function, whereas cardiomyocyte-specific increased activity of p38 and JNK results in cardiac fibrosis and ventricular dilation (Bueno et al., 2000; Iwaki et al., 1990).

During cardiac hypertrophy, MAPK pathways intervene in transcriptional regulation via phosphorylation-dependent modulation of transcription factors including NFAT, Elk, SRF and GATA4 (Sanna et al., 2005). Preceding expression of hypertrophic genes, ERK-dependent activation of an immediate early gene (IEG) response is observed in cardiomyocytes. Specifically, IEG expression is rapidly activated in cultured rat neonatal ventricular cardiomyocytes in response to stimulation with hypertrophic agonists, and in vivo following pressure overload (Archer et al., 2017; Iwaki et al., 1990; Izumo et al., 1988). This response is initiated through phosphorylation-dependent activation of the AP-1 family of transcription factors, which promote the induction of IEG expression within minutes of the initiating cue (Balmanno and Cook, 1999; Gille et al., 1992; Karin et al., 1997). Proto-typical IEG include members of the FOS (c-FOS, FOSB, FRA-1 and FRA-2), Jun (JUNB, JUND and c-JUN) and activating transcription factor (ATF; ATFa, ATF2, LRF1/ATF3, ATF4 and B-ATF) families of basic-leucine zipper transcription factors (Eferl and Wagner, 2003). Heterodimers of Fos and Jun associate with ATFs to form the AP-1 transcription factor complex (Glover and Harrison, 1995). The actions of AP-1 transcription factors are also mediated via direct interactions with other transcription factors, many of which, including NFκB and NFAT are involved in collaborations in regulating gene expression in many non-cardiac systems (Chen et al., 1998; Torgerson et al., 1998; Yang et al., 2010). The AP-1 complex is also involved in cardiac hypertrophic responses. This role is clearly illustrated in in vitro and in vivo experiments in which AP-1 activity is suppressed through expression of dominant negative JUN (DN-JUN; also known as TAM67) or of

the endogenous AP-1 inhibitor JUND (Hilfiker-Kleiner et al., 2006; Kim-Mitsuyama et al., 2006; Takeuchi et al.). Moreover, muscle-specific knockout of c-Jun results in a loss of the initial compensatory phase of the pathological hypertrophic response and a progression to cardiac dilation, indicating a requirement for c-Jun in the initial phase of the cardiac hypertrophic response (Tachibana et al., 2006; Windak et al., 2013). Taken together, these results indicate that despite certain specific roles for different IEG, the AP-1 transcription factor complex fulfils important and complex functions in hypertrophic remodelling.

Although ERK activation and IEG induction in cardiomyocytes are highly correlated, the mechanism by which these events are coupled during induction of cardiomyocyte hypertrophy is not resolved. In other systems, MAPK activation leads to a nucleosomal response at IEG loci that involves phosphorylation and acetylation of serine and lysine residues respectively in the histone H3 NH_2-terminal tail (Clayton et al., 2000; Dyson et al., 2005). Phosphorylated histone H3 in turn recruits scaffolding proteins such as 14-3-3 family members, downstream transcriptional regulators and chromatin remodelling factors to bring about gene expression changes. The absence of a consensus site for ERK1/2 phosphorylation in the NH_2-terminus of histone H3 would suggest that its phosphorylation is not directly via ERK1/2 but a downstream kinase. A candidate for this activity is the family of nuclear-localised mitogen and stress activated kinases (MSK1/2), which have been reported to mediate histone H3 phosphorylation (Duncan et al., 2006; Soloaga et al., 2003a). MSKs are nuclear-localised kinases comprising N- and C-terminal kinase domains separated by a flexible linker peptide. After an initial phosphorylation event by upstream MAPK including ERK1/2, MSKs undergo autophosphorylation, leading to full activation (Malakhova et al., 2009; McCoy et al., 2005). A potential role for MSK in cardiac remodelling is also reported.

Specifically, MSK1 and the highly homologous kinase MSK2 are both expressed in the heart and are activated in response to hypertrophic stimuli (Deak et al., 1998a; Markou et al., 2004, 2009). A requirement for MSK in the induction of the hypertrophic response has also been proposed to involve downstream activation of the histone acetyltransferase cAMP binding protein (CREB) (Markou et al., 2009). The nanomolar efficacy of the Ro318220 compound for MSK targets RSK2, PKC isoforms and S6 kinase used in the aforementioned study may preclude the drawing of this conclusion (Bain et al., 2007). Moreover, the contribution of the nucleosomal response, which in other cell types appears to be central to the action of MSK and the induction of IEG expression, was not examined.

Here, we determined that MSK1/2 activated downstream of ERK1/2 promoted the phosphorylation of histone H3 S28 (pH3S28), which in turn recruits AP-1 factors, c-FOS and c-JUN along with the chromatin remodeller BRG-1 to IEG promoters, inducing transcription. Moreover, and supporting the physiological importance of this pathway, MSK was required for the hypertrophic response both *in vitro* and *in vivo*. Further, the ERK1/2-MSK1/2-pH3S28 molecular axis was conserved in human.

Together our data identify a key and missing component in the signalling pathway that transduces the activation of GPCRs by pathological pro-hypertrophic mediators in cardiomyocytes to the induction of hypertrophic remodelling.

Results

ERK1/2 activity is required for the induction of cardiomyocyte hypertrophic gene expression by ET-1 in vitro.

MAPK signalling pathways, IEG induction and AP-1 transcription factor engagement contribute to the hypertrophic remodelling of cardiomyocytes (Archer et al., 2017). To examine the mechanisms underlying induction of IEG expression, the signalling pathways involved and their relationship to cellular hypertrophic responses were analysed in in vitro and in vivo models following acute exposure to established inducers of pathological hypertrophy.

Consistent with findings from our laboratory and elsewhere, brief exposure of neonatal rat ventricular myocytes (NRVMs) to the GPCR agonist endothelin-1 (ET-1) resulted in a classical hypertrophic response associated with increases mRNA levels of Anf/*Nppa* and Bnp/*Nppb*, in cell size and in the number of cells positive for perinuclear Anf protein (Figure 1A-C and S1A). Alongside this hypertrophic response, the expression of IEGs including *c-Fos* and *c-Jun*, was upregulated in ET-1 stimulated NRVMs (Archer et al., 2017) (Figure 1D, Figure S1B). These effects of ET-1 on both induction of hypertrophy and IEGs were prevented by inhibition of the MAPK pathway with PD184352 (PD, an inhibitor of the direct upstream kinase of ERK1/2, MEK1/2; Figure S1C) (Archer et al., 2017; Heineke and Molkentin, 2006) (Figure 1A-D). The efficacy of PD in preventing ERK1/2 activation (and hence MAPK pathway activation) was confirmed by immunoblotting, which showed a loss of the phosphorylated active form of ERK, pERK1/2, which was elevated in ET-1 stimulated NRVMs (Figure S1D). Baseline pERK1/2 in non-stimulated cells was also decreased following PD (Figure S1D).

Consistent with the role of MAPK signalling to AP-1 in hypertrophy induction, a MAPK-dependent increase in activity of a luciferase-based AP-1 reporter was observed in ET-1 stimulated NRVMs (Figure 1E). Further, inhibition of AP-1 activity by adenoviral-mediated expression of dominant negative Jun (DN-Jun) abrogated the ET-1 stimulated increases in cell surface area and *Nppa* mRNA (Figure 1F-G).

Together, these data confirm that a pathway involving ERK1/2, IEG induction and AP-1 activity is engaged and required for the immediate early hypertrophic response to ET-1.

Endothelin-1 stimulates ERK-dependent phosphorylation of Histone H3 Serine 28 specifically.

The nucleosomal response – a term coined to link histone phosphorylation and IEG induction - is reported to be indissociable from ERK1/2 activity in a number of cell contexts. We therefore determined whether this nucleosomal response was engaged during ET-1 stimulated IEG induction in NRVM. Levels of histone H3 phosphorylated at Ser 10 and Ser 28 (pH3S10 and pH3S28) were quantified in histones acid-extracted from NRVMs exposed to ET-1. Consistent with the time-course of *c-Fos* induction, ET-1 promoted a significant increase in H3S28 phosphorylation at 10 min, which was not increased further at 30 min post ET-1 application (Figure 2A). Notably, the ET-1-stimulated increase in H3S28 phosphorylation was ERK pathway dependent, as shown by the loss of the response to ET-1 in cells treated with PD (Figure 2A). Neither ET-1 nor PD significantly affected H3S10 phosphorylation (Figure 2A).

The stimulation of H3S28 phosphorylation by hypertrophic agonists was next measured in vivo. To this end, cardiomyocyte H3S28 phosphorylation was analysed in

adult rats subsequent to 15 min infusion with sub-pressor levels of ET-1 via the jugular vein (Archer et al., 2017; Beyer et al., 1994; Dyson et al., 2005). Responses to the synthetic β-adrenergic agonist isoproterenol (Iso), which is often used chronically to induce pathological cardiac remodelling was also determined (Boluyt et al., 1995; Liu et al., 2009). Both ET-1 and Iso induced a significant increase in pH3S28 in cardiomyocyte nuclei (demarcated by Pcm-1 staining) in heart sections from rats infused with ET-1 and Iso (Figure 2B). Concurrent with increased pH3S28 in this in vivo model, mRNA expression of IEGs was induced following 15 min stimulation (Figure 2C and S2A). Supporting the pro-hypertrophic effect of these infusions with ET-1 or Iso, expression of the classic hypertrophy-associated foetal gene programme, including *Nppa/Anf* and *Nppb/Bnp* was also induced in these animals (Figure S2B).

To probe whether IEG promoters were phosphorylated at histone H3 during this intervention, chromatin immunoprecipitation (ChIP) experiments were performed. Chromatin was precipitated using antibodies against phosphorylated H3S28 and product detected by qPCR using primer pairs targeting the c-*Jun* and c-*Fos* promoters, as shown in the cartoons (Figure 2D). Notably, consistent with the increase in phosphorylated H3S28 detected by immunoblotting and immunofluorescence staining of bulk histones, ChIP enrichment for pH3S28-associated IEG promoters was substantially increased following 15 min ET-1 or Iso infusion (Figure 2D).

MSK1/2 is activated following ET-1 stimulation in an ERK1/2 dependent manner and is required for IEG expression

Although ERK activation is required for ET-1 dependent phosphorylation of histone H3 at S28, the absence of consensus sequences for its phosphorylation of H3 would suggest that it is not the responsible histone-kinase. Rather, ERK activates a

downstream effector kinase that in turn phosphorylates histone H3. A candidate for this action is the mitogen and stress-activated kinase (MSK1/2), which has been shown in other tissue contexts to phosphorylate H3S28 (Soloaga et al., 2003a). While MSK1/2 activation following hypertrophic stimulation is reported in cardiomyocytes, it has not been shown to play a role in histone phosphorylation and IEG induction. To establish whether MSK1/2 was engaged during ET-1 stimulation of cardiomyocytes and whether ERK activity was involved, levels of MSK1 phosphorylated at S376, a phosphorylation event required for activity, were analysed by immunoblotting of lysates prepared from NRVM stimulated with ET-1-stimulated ± PD (Figure 3A). As shown in the immunoblot and accompanying densitometric analysis, ET-1 stimulated an increase in pMSK that was sensitive to MEK/ERK pathway inhibition with PD (Figure 3A). Importantly, using the in vivo model described earlier, an increase in pMSK was also detected in cardiomyocyte nuclei in heart sections from rats infused with ET-1 or Iso for 15 min (Figure 3B). Together, these experiments indicated that hypertrophic agonists stimulate a rapid phosphorylation of MSK in cardiomyocytes that is dependent on activation of MEK/ERK signalling.

Experiments were next conducted to investigate the functional role of MSK in the nucleosomal response to ET-1 in cardiomyocytes. Owing to the lack of availability of specific and sensitive pharmacological agents targeting MSK1/2, a molecular approach was adopted to manipulate its activity (Bain et al., 2007). To this end, adenoviruses were first employed. MSK1 signalling was enhanced through overexpression of wild-type MSK1 (WT-MSK), whilst endogenous MSK1 was inhibited by expression of a D565A kinase dead mutant of MSK1 that acts in a dominant–negative fashion (DN-MSK1) (Deak et al., 1998a). Owing to shared regulatory mechanisms of MSK1 and MSK2, DN-MSK1 would be expected to inhibit activity of

both kinases, overcoming possible redundancy (Zhong et al., 2001). Immunofluorescence analysis demonstrated that adenovirally-expressed FLAG-tagged WT- and DN-MSK1 were both localised to the nucleus in NRVMs (Figure 3C). Overexpression of the WT and DN-MSK1 proteins at equivalent levels was confirmed by immunoblotting using an antibody directed against their NH_2-terminal FLAG epitope (Figure 3D). Overexpression of WT-MSK1 produced an increase in baseline MSK1 phosphorylation whilst DN-MSK1 prevented the activation of endogenous MSK1 in response to ET-1, consistent with a dominant negative effect (Figure 3D). Neither overexpression of WT-MSK1 or DN-MSK1 affected ERK1/2 activation by ET-1, indicating that effects of these strategies to modify MSK activity are not mediated via altered ERK1/2 activity but by MSK1 itself (Figure 3D). The consequences of WT and DN-MSK1 expression on ET-1 stimulated histone H3S28 phosphorylation were next measured. Notably, both ET-1 and overexpression of WT-MSK1 elevated levels of pH3S28 in NRVMs, whereas expression of DN-MSK1 prevented the ET-1 stimulated increase in pH3S28 (Figure 3E), thereby demonstrating the requirement for MSK activity for H3S28 phosphorylation during the hypertrophic response to ET-1.

Whether the effect of WT and DN-MSK on MSK activation in ET-1 stimulated NRVM translated to an effect on IEG induction and hypertrophic responses was next examined (Figure 3F-G). NRVM expressing WT-MSK expression exhibited a significant elevation in *c-Fos* expression compared to control, which was not increased further by 10 min exposure to ET-1 (Figure 3F). Consistent with its effects on kinase activation and H3S28 phosphorylation, DN-MSK1 expression significantly inhibited ET-1 stimulated *c-Fos* induction. WT-MSK expression also had a significant effect on cell hypertrophy, stimulating an increase in cell area in the absence of ET-1 (Figure 3G). WT-MSK1 did not promote a significant increase in *Nppa* mRNA. Notably DN-MSK1

expression suppressed hypertrophic responses in NRVM exposed to ET-1 for 24 h, with a significant inhibition of the ET-1 stimulated increases in *Nppa* mRNA and in cell size observed when compared to controls (Figure 3G). Further supporting the role of MSK in histone H3 S28 phosphorylaiton, IEG induction and hypertrophy, abrogation of ET-1 stimulated increases in H3S28 phosphorylaiton, *c-Fos* and *Nppa* mRNA expression were also observed in ARVM (Figure S3A-C).

Having validated that suppression of MSK activity via DN-MSK1 expression could prevent ET-1 stimulated phosphorylation of histone H3S28, *c-Fos* induction and hypertrophic responses, we next probed the requirement for MSK for ET-1 stimulated phosphorylation of H3S28 at IEG promoters. To this end, ChIP experiments were carried out in NRVMs expressing DN-MSK1 or empty vector control that were exposed to ET-1 or vehicle for 10 min. Importantly, DN-MSK1 prevented the ET-1-stimulated increase in pH3S28 specifically at IEG promoters (Figure 3H). In these experiments, the ET-1 stimulated ChIP enrichment of c-*Jun* and c-*Fos* promoters was lost in NRVM overexpressing DN-MSK1 (Figure 3H).

To complement the experiments using DN-MSK, the requirement of MSK activity for ET-1 induction of *c-Fos*, *Msk1* mRNA expression was tested by knocking down its expression using small interfering RNA (siRNA). Using this approach, ~60 % reduction in *Msk1* mRNA was achieved compared to NRVM transfected with scrambled control siRNA (Figure S3C). In Msk1 siRNA knockdown (siMsk1) NRVMs, ET-1 stimulated induction of *c-Fos* was significantly blunted after 10 min exposure (Figure S3D). Moreover, siMsk1 prevented ET-1 stimulated induction of hypertrophic gene expression (Figure S3E).

Together, these data generated using siRNAs and adenoviruses to manipulate both MSK activity and expression not only indicate that H3S28 is a substrate for MSK1 but

also that MSK1 is the kinase responsible for the phosphorylation of H3S28 and induction of *c-Fos* expression in cardiomyocytes stimulated with ET-1. Moreover, our data shows that these events are required for the hypertrophic response of cardiomyocytes.

MSK1-mediated phosphorylation of H3S28 recruits BRG1, a component of the SWI/SNF family of chromatin remodelers to IEG loci

Previous studies have reported a requirement for the BRG1 (encoded by gene *SMARCA4*) component of the BAF (BRG1/BRM-associated factor 60; BAF60) ATP-dependent SWI/SNF chromatin remodelling complex in induction of IEG expression and Myh isoform switching in pathological cardiac remodelling (Deak et al., 1998b; Hang et al., 2010). The role of Brg1 in IEG induction and hypertrophic remodelling was therefore tested. Consistent with previous studies, knock down of Brg1 with siRNA prevented isoform switching between *Myh6* and *Myh7*, associated with induction of pathological hypertrophy, and abrogated *c-Fos* induction in ET-1 stimulated NRVMs (Figure S3F-G). Having shown the involvement of Brg1 in ET-1 responses in NRVM, whether phosphorylation of H3S28 affected Brg1 occupancy at IEG promoters was next investigated. To this end, ChIP experiments were performed on NRVMs expressing DN-MSK1 ± ET-1, as in Figure 3H but using an antibody directed Brg1. Notably, as shown by greater ChIP enrichment, ET-1 stimulated increases in association of Brg1 with both the *c-Jun* and *c-Fos* promoters in NRVMs (Figure 3I). Brg1 recruitment was however prevented in DN-MSK expressing NRVMs. Further supporting these in vitro data, Brg1 was also enriched at the *c-Jun* and *c-Fos* promoters in chromatin prepared from hearts from Wistar rats infused with ET-1 or Iso for 15 min (Figure 3J).

Collectively, these data demonstrate that MSK-mediated phosphorylation of histone H3S28 at the promoter regions of IEGs is a necessary event for the recruitment of the chromatin remodelling complex to these promoters required for IEG expression and hypertrophic remodelling subsequent to GPCR stimulation.

MSK1/2 expression is required for the hypertrophic response in vivo.

The data above indicate a role for MSK in the induction of hypertrophic responses in vitro and that the MSK/pH3S28/Brg1/IEG pathway is acutely engaged following neurohumoral stimulation in vivo. The requirement for MSK1/2 for activation of this pathway and induction of hypertrophy was next examined in vivo using a mouse model in which both alleles of *Msk* had been deleted by homologous recombination (*Msk1/2*$^{-/-/-}$; *Msk* KO) (Wiggin et al., 2002a). Specifically, wild type (WT) and *Msk* knockout (KO) mice were subjected to osmotic mini-pump infusion of Iso for one week, after which the activation of the MSK pathway and hypertrophy induction was measured. During this one week infusion, the initial adaptive remodelling associated with pathological hypertrophy would be expected.

The activation of the MSK/pH3S28/Brg1/IEG pathway axis during the one week Iso infusion and how it was affected by loss of Msk1/2 was first assessed. As expected for the *Msk* KO mice, *Msk1* and *Msk2* transcripts were absent in heart tissue in this mouse (Figure 4A). *Msk1* and *Msk2 mRNA levels* were also measured in the iso infused WT mice and found to be significantly upregulated after 1 week (Figure 4A). Notably, Iso-infused WT mice exhibited significant increases in expression of IEGs including *c-Fos* and *c-Jun* and in line with its role in IEG induction of *Smarca4* (the gene encoding Brg1) (Figure 4B-C). Consistent with the importance of MSK1/2 in the IEG response,

Iso induction of *c-Fos, c-Jun* and *Smarca4* expression was reduced in these mice when compared to similarly treated WT controls (Figure 4B-C). Levels of nuclear pMSK and pH3S28 (demarcated by Pcm-1 or Nesprin perinuclear staining (Thienpont et al., 2017) in cardiomyocytes in sections prepared from Iso-infused WT and KO animals were also significantly lower in KO animals than WT at baseline and were not affected by Iso, indicating inactivation of the MSK/pH3S28 pathway (Figure 4D-E). While significantly higher than in KO at baseline, no significant effect of Iso on pMSK or pH3S28 was however observed in WT cardiomyocytes.

We tested whether upregulation of IEGs, *Smarca4* and *Msk*1/2 was a feature of other models of hypertrophic remodelling. In line with these findings in Iso infused mice, an upregulation of IEGs, *Smarca4* and of *Msk1/2* was detected in cardiomyocytes from rats subjected to constriction of the ascending aorta (AB) for 6 weeks (a model of pathological hypertrophy) (Thienpont et al., 2017) (Figure S4A). Indicative of a specific role of this IEG response to pathological cardiac remodelling, no such upregulation was detected in cardiomyocytes from rats subjected to treadmill training for 6 weeks, which exhibited physiological cardiac remodelling, with a similar degree of hypertrophy as the AB rats (Thienpont et al., 2017) (Figure S4A). *Msk1* and *2* mRNA levels were also increased in NRVMs after 24 h of ET-1 stimulation (Figure S4B).

Having confirmed the engagement of the MSK/pH3S28/Brg1/IEG pathway in Iso-infused mice, and the requirement for MSK1/2 for phosphorylation of H3S28 and induction of IEG, hypertrophic remodelling was assessed in these animals. Cardiac function and geometry was measured in vivo by 2D echocardiography prior to the start of the experiment (baseline) and after one week of Iso infusion. In line with the reported lack of an overt phenotype in *Msk* double KO mice, no differences in cardiac function, indicated by fractional shortening (FS) or of posterior wall thickness (PWd) were

413 detected between control WT and KO animals at baseline (Figure 4F and S4C).
414 Following one week Iso infusion, whereas control mice exhibited significant increases
415 in PWd and FS, typical of the initial stages of pathological hypertrophic remodelling
416 (Selvetella et al., 2004), these responses to Iso were absent in *Msk* KO mice (Figure
417 4F-G and S4C).

418 The hypertrophic response to Iso infusion was also assessed by RT-qPCR analysis of
419 components of the foetal gene program. As would be expected, Iso infusion resulted
420 in increased expression of *Nppa*, *Nppb* and *Myh7* in WT mice (Figure 4H). The
421 expression of these hypertrophic markers was not however induced following Iso
422 infusion in *Msk* KO mice, thereby supporting the requirement for Msk for the
423 hypertrophic response observed in vitro.

424 Fibrosis is a feature of pathological hypertrophy, including following Iso infusion that
425 contributes to disease progression. Histological analysis of LV tissue sections revealed
426 a significant increase in interstitial fibrosis following Iso infusion in control mice that
427 was absent in the *Msk* KO mice (Figure 4I and S4D). Supporting the histology analysis,
428 *Col1a1* mRNA was substantially increased in Iso infused WT mice that was absent in
429 similarly treated *Msk* KO mice (Figure 4J).

430 Fibrosis is a natural response to increased cardiomyocyte death in the myocardium.
431 Given the association between cardiomyocyte viability and the activity of MAPK
432 pathways, we assessed whether reduced cell death was contributing to the protective
433 effects of Msk KO. TUNEL staining of heart sections revealed a significant Iso-
434 dependent increase in cell death in WT mouse hearts that was not observed in *Msk*
435 KO mice (Figure S4E). Baseline cell death was similar between WT and *Msk* KO
436 mouse hearts. The expression of key anti- and pro-apoptotic mediators was analysed

(Figure S4F and G). Expression of executioner caspases 3 and 9 (*Casp3* and *Casp9*) of apoptosis and of *Bax*, a pro-apoptotic BH3 only family member, were increased following Iso in WT mice, whereas their expression was not induced in the *Msk* KO mouse (Figure S4F). Notably, Bcl2, which exhibits anti-apoptotic activity, was increased in the *Msk* KO mouse following Iso infusion (Figure S4G).

Together these data show that consistent with that observed in vitro, MSK activity is required for the induction of hypertrophy in vivo, and that in its absence, hearts are protected from pathological insult.

The MSK1/2/pH3S28/BRG1/IEG axis is engaged in human hypertrophic remodelling

Having shown an important role of MSK1/2 in IEG and hypertrophy induction in cellular models and in vivo in rodents, we analysed whether the MSK1/2/pH3S28/IEG axis was conserved in GPCR responses and hypertrophic remodelling in human. To this end, the activation of MSK and phosphorylation of H3S28 following application ET-1 and Iso was first analysed in acutely isolated ventricular cardiomyocytes from explanted non-failing donor hearts. The involvement of MAPK activity was also tested. Stimulation of human cardiomyocytes resulted in a significant increase in levels of pMSK and pH3S28 (Figure 5A-B). Consistent with our findings in rat ventricular cardiomyocytes, these phosphorylation events were abrogated by inhibition of the ERK1/2 pathway with PD.

To gain insight into the involvement of MSK and IEG in human disease, the expression of MSK1/2, IEGs and early response gene target *SMARCA4* was compared between cardiomyocyte nuclei purified from healthy and hypertrophic human hearts. As in

rodents, expression of MSK1/2, IEG components of the AP-1 transcription factor and SMARCA4 were substantially upregulated in hypertrophic cardiomyocytes (Figure 5C-E). We next analysed pH3S28 in the promoters of *c-FOS, C-JUN* and *SMARCA4* by ChIP. Notably, pH3S28 enrichment was observed at all three promoters in hypertrophic compared with healthy control hearts (Figure 5F-G).

Together, these data show conservation of the MSK pathway to IEG induction in human hearts and support our hypothesis that the MSK/pH3S28/IEG pathway is necessary to bring about the initial stages of the pathological hypertrophic response in cardiomyocytes (Figure 6).

Discussion

MAPK regulation of immediate early gene activity and expression is key to stress-mediated induction of cardiac hypertrophic responses. Here we identified MSK1/2, a kinase activated downstream of ERK1/2, as being necessary for the initiation of IEG expression in response to pathological hypertrophic cues. MSK1/2 elicited this response through phosphorylation of histone 3 at Ser 28 allowing recruitment of the ATP-dependent chromatin remodeller, Brg1. In the absence of this response, hypertrophic gene expression and cardiac remodelling was attenuated. Notably, live-cell functional assays and analysis of post-mortem human hypertrophic hearts revealed that this pathway was conserved in humans. These data are summarised in the cartoon in Figure 6.

The hypertrophic response of the pathologically stressed myocardium is mediated through an extensive remodelling of the cardiomyocyte transcriptome (Selvetella et al., 2004; Song et al., 2012). Contributing to the initiation of this process as well as being required for its manifestation are AP-1 transcription factors, that comprise

heterodimers of, but not restricted to, the proto-typical IEGs c-FOS and c-JUN (Chiu et al., 1988; Hess et al., 2004). Through their signal responsive phosphorylation, AP-1 are acutely activated in response to hypertrophic stimuli and upon phosphorylation associate with cognate response elements in the promoters of their encoding genes as well as numerous other targets, thereby promoting a rapid induction of their expression. Consistent with previous work from our laboratory and others and this established paradigm for AP-1 activity in the heart, we show here that the expression of these IEGs is increased within minutes of exposure of cells to hypertrophic agonists, both in vitro, and importantly in vivo (Archer et al., 2017). As revealed by use of dominant negative AP-1 components shown here and in previous studies, the induction of these early response genes, which include many transcription factors, is important in mediating later phases of the hypertrophic response (Hilfiker-Kleiner et al., 2006; Petrich et al., 2003).

ERK1/2 in the heart

Activation of the ERK1/2 MAPK pathways is a conserved feature of many hypertrophic stressors. This signalling cascade is activated following receptor engagement at the plasma membrane and culminates in induction of hypertrophic gene expression. As we show here and described elsewhere, expression of immediate early genes occurs in vitro and in vivo within minutes of exposure to hypertrophic agonist, and is the first transcriptional readout of MAPK activation. Indeed, we show that ERK1/2 activation mirrors the temporal profile of IEG induction. Moreover, in the absence of ERK activity, hormone stimulated AP-1 activation, IEG induction and expression of markers of hypertrophy in myocyte cultures is prevented in vitro and in vivo (Liu et al., 2016).

Notably, while ERK and IEG activity peak proximal to the initiating stimulus, despite a lack of detectable activity subsequent to this peak, ERK inhibition prevents hypertrophic gene expression (Archer et al., 2017).

While we, as others, show an involvement of ERK1/2 and activation of IEGs in the mechanism underlying pathological hypertrophic remodelling, the role of ERK1/2 in hypertrophy in vivo is complex. Whereas in vivo overexpression of ERKs is not sufficient to induce a hypertrophic response, overexpression of its direct upstream kinase MEK induces a concentric hypertrophic response (Mutlak and Kehat, 2015). However, overexpression of the small GTPase protein Ras, which lies between GPCR activation and ERK activation, results in cardiomyopathy (Wu Guangyu et al., 2001). Recent elegant strategies involving conditional or tissue specific manipulation of each isoform to overcome embryonic lethality of the genetic KO now provide a clearer view of the contribution of this pathway to the cardiac hypertrophic response. Loss of ERK2, which represents 50-70 % of ERK activity in the heart attenuates the initial compensatory phase of the hypertrophic response and a direct progression to a cardiomyopathic phenotype. Significantly, this cardiomyopathic phase is associated with substantial cardiomyocyte death, which would indicate that ERK2 elicits a protective anti-apoptotic effect upon the cardiomyocyte. While initial reports suggested no impact of *Erk1/2* cardiac KO ($ERK1^{-/-}ERK2^{+/-}$) on stress-induced cardiac growth, a later study demonstrated that this intervention, along with cardiac-restricted overexpression activated MEK1, resulted in a switch from concentric to eccentric (lengthening) cardiomyocyte growth (Bueno et al., 2000; Purcell et al., 2007). Ablation of ERK1/2 signalling in the heart by cardiac-specific transgenic mice overexpressing DUSP6 present with a predisposition to developing a dilatory phenotype and increased cardiomyocyte apoptosis (Purcell et al., 2007). Surprisingly, cardiomyocyte-specific

loss of *Erk2* in mice did not affect physiological cardiac remodelling in response to 4 weeks of swimming training, indicating independent pathways for adaptive hypertrophy in response to pathological or physiological stimuli (Ulm et al., 2014).

These diverse data from these different experimental models are perhaps not surprising given the complex regulation of this pathway, involving feedback at multiple levels that act to prevent constitutive activity. Together, these experimental findings suggest that ERK signalling contributes to acute, adaptive hypertrophic growth while repressing maladaptive growth thereby protecting the heart from maladaptive remodelling and progression to failure. A similar role is also suggested of certain AP-1 components where in their absence, the hypertrophic response is less adaptive in nature (Windak et al., 2013).

MSK in the heart

As indicated above, ERK1/2 signalling is critical for transduction of hypertrophic cues to activation of IEG expression and induction of hypertrophy. Moreover, ERK1/2 phosphorylates hypertrophy-related transcription factors to modulate the activation. Phosphorylation of histone H3 at S10 and S28 has also been described as key events in the pathway indissociably linking MAPK activation and induction of IEG expression in response to mitogenic stimulation (Clayton and Mahadevan, 2003; Clayton et al., 2000). MAPK cannot however directly phosphorylate H3S28 and S10 but act via an intermediate kinase, which in fibroblastic cells was identified as the mitogen and stress activated kinase MSK1/2. MSK1/2 are promiscuous nuclear serine/threonine proteins. MSK is activated either through ERK1/2 or p38 MAPK cascades, resulting in phosphorylation of the MSK C-terminal Ca^{2+}/calmodulin-dependent protein kinase

559 (CaMK)-like domain, leading to a positive feed forward autophosphorylation event at
560 the N-terminal AGC-like kinase domain (Roux and Blenis, 2004). The phosphorylated
561 activated N-terminal domain then phosphorylates other substrates, including histone
562 H3. Our study provides the first evidence for a role for MSK in promoter histone H3
563 phosphorylation and IEG induction in cardiomyocytes. Although the necessity for IEG
564 activation in the mitogenic stress response mediated through CREB and ATF has been
565 described in cultured fibroblasts isolated from *Rsk2* or *Msk1/2* double KO mice
566 (Soloaga et al., 2003b), the data presented here are the first demonstration that
567 phosphorylation of H3S28 by MSK is required for IEG activation and mounting of the
568 cardiomyocyte hypertrophic response. The specific role for MSK1/2 in responding to
569 stress stimuli is consistent with the lack of overt phenotype in *Msk1/2* double KO mice
570 (Wiggin et al., 2002b).

571 Histone H3 Ser 28 phosphorylation at IEG promoters is an important step in the
572 induction of their expression. This phosphorylation event results in increased
573 recruitment of BRG1, a component of the SWI/SNF remodelling complex to chromatin
574 (Hang et al., 2010). Appropriate localisation of this complex to chromatin is likely a key
575 step in bringing about the required transcriptional response. Notably, BRG1 is an
576 important mediator of chromatin remodelling and transcriptional responses in cardiac
577 development and disease. Indeed, BRG1 together with HDAC and PARP is recruited
578 to the *Myh6/7* locus and is involved in bringing about the isoform switching of myosin
579 heavy chain during cardiac maturation and in response to stress. The lack of Brg1
580 recruitment following DN-MSK expression described here would support these
581 previous observations. Based on our data, we propose that H3S28 phosphorylation by
582 MSK is an initial step in mediating this hypertrophic response. The recruitment of BRG1
583 further contributes to modulation of the epigenetic landscape of the heart through

584 recruiting factors including EZH2 to acetylate H3K27 at enhancers of the mesoderm
585 and for Polycomb-mediated repression of non-mesodermal genes (Gehani et al.,
586 2010). Such a role for MSK-mediated phosphorylation of H3S28 is described in
587 neuronal differentiation, where MSK1/2 phosphorylates and targets H3S28 in
588 promoters with Polycomb repressor complex 2 (PRC2) – bound methylated H3K27,
589 thereby displacing PRC2 for gene activation (Gehani et al., 2010). H3K27me3 is also
590 lost at activated gene promoters in hypertrophy and disease in cardiomyocytes
591 (Gilsbach et al., 2014; Thienpont et al., 2017). Whether loss of this mark is associated
592 with gain of H3S28 phosphorylation is not determined in cardiomyocyte transcriptional
593 responses, although elsewhere, phosphorylation of H3S28 has been shown to
594 displace the PRC complex allowing H3K27 acetylation (Kim et al., 2012). Together,
595 these data suggest that MSK-mediated phosphorylation of H3S28 is important in
596 bringing about epigenetic changes underlying cardiac development and in the
597 responses to hypertrophic cues.

598 Phosphorylation of histone H3 has previously been described in cardiomyocytes, albeit
599 in the context of a bona fide hypertrophic response. In chronic remodelling in response
600 to sustained sympathetic activation, CaMKII was found to bind directly and
601 phosphorylate H3S28. In end-stage heart failure as well as in a murine model, CaMKII-
602 mediated H3S28 promoter activates at adult haemoglobin gene expression
603 (Saadatmand et al., 2019). Whether this particular mechanism is protective or
604 contributes to the pathological phenotype is undetermined. Importantly, CaMKII was
605 found necessary for sustained elevation of global pH3S28, with major differences
606 compared with control seen after 24 h catecholaminergic stimulation (Saadatmand et
607 al., 2019). While CaMKII may indeed play a role at certain gene loci, the decrease in
608 H3S28 phosphorylation in *Msk* KO animals, suggests that MSKs make an important

609 contribution to maintaining phosphorylation of H3S28, particularly at IEG loci shown
610 here, during disease remodelling. CaMKII is also shown to phosphorylate H3S10
611 leading to the induction of cardiac foetal genes (Awad et al., 2013). Notably, in the
612 latter study, no CaMKII dependent phosphorylation of H3S28 was detected. The
613 nuclear localisation of this kinase together with its identified role in HDAC
614 phosphorylation provides a mechanism to remodel chromatin in a manner optimal for
615 stimulation of MEF2-dependent gene expression during hypertrophic remodelling
616 (Awad et al., 2013; Backs et al., 2006). CaMKII-associated pH3S10 is also sustained
617 in end-stage heart failure (Awad et al., 2015). As we did not detect a robust change in
618 H3S10 phosphorylation in NRVMs exposed to hypertrophic stimuli, we did not examine
619 phosphorylation of this residue in disease in vivo. Together, CaMKII phosphorylation
620 of H3S10 and H3S28 and H3S28 phosphorylation by MSK may underlie a mechanism
621 that permits different stimuli at different phases of their action to selectively control the
622 expression of discrete panels of target genes.

623 Consistent with studies elsewhere, we show that MSK lies downstream of ERK1/2,
624 requiring ERK activity for function (Markou and Lazou, 2002) (Figure SB). MSK is also
625 modified by p38 MAPK, which has been proposed to be required in addition for ERK1/2
626 for activation and in mediating pathological cardiac stress responses. Further, MSK is
627 proposed to induce hypertrophic responses via CREB in a manner that also requires
628 PKA (Markou et al., 2004). These studies were however constrained by the poor
629 pharmacology of MSK with drugs used targeting PKC and PKA in the nM range (Alessi,
630 1997). Since in agreement with other studies, ERK inhibition was sufficient to prevent
631 MSK activation and its regulation of effectors, we did not probe further the role of p38.
632 Notably, as well as showing increased phosphorylation of sites indicative of its
633 activation, *MSK1/2* gene expression was induced in response to hypertrophic

stimulation both in vitro and in vivo. *MSK1/2* expression was also maintained in more chronic situations, further underlining the importance of this kinase in early responses to stress as well as in potentially sustaining it function. The persistence of IEG expression in the 6 week rat model of hypertrophic remodelling and in human disease may support this notion.

Other targets of MSK involved in the cardiac hypertrophic response have been described. The first substrate of MSK identified was the cAMP-Responsive Element-Binding Protein (CREB) transcription factor, which binds cAMP response DNA elements (CRE), associating with the histone acetyltransferase CREB-binding protein (CBP/P300) to activate transcription. CREB itself is also phosphorylated by a number of different kinases, including protein kinase A (PKA) (Johannessen et al., 2004). The role of MSK-activated CREB in vivo is controversial. Several studies have demonstrated that PKA- but not MSK-mediated CREB phosphorylation leads to CBP or p300 recruitment (Kasper et al., 2011). Cardiac-specific expression of a dominant negative form of CREB (DN-CREB) leads to a dilated cardiomyopathy phenotype (Watson et al., 2010). Given the extreme phenotype of DN-CREB in contrast to the relatively benign *Msk1/2* double KO, it is likely that normal CREB activity is independent of MSK in the heart. Related to its role in the nucleosomal response, MSK phosphorylates high mobility group 14 protein (HMG-14). This protein associates with phosphorylated H3 at activated promoters (Soloaga et al., 2003b). Its role in chromatin remodelling remains elusive and its relationship with MSK and H3 phosphorylation remains however, to be determined (Phair and Misteli, 2000).

Pharmacology of MSK for therapeutic targeting

The lack of a significant cardiac phenotype of *Msk1/2* KO suggests a limited role of MSK in the basal activity of cardiomyocytes. The stress-specific function of MSK may endow it however with possessing the necessary qualities of being therapeutically targetable. To date, no highly specific drugs suitable for in vivo use are available and those that are show equivalent efficacy at other important kinases including PKC and PKA, the use of which would preclude identification of MSK mechanisms of action and role in the heart. Specific inhibitors of kinases upstream of MSK, including members of the ERK/MAPK pathway have also been employed. The role of these kinases in the baseline activity of the heart is more significant making them less ideal targets for therapy.

Conclusion

Our data identified MSK as the missing link between ERK/MAPK activation, histone H3S28 phosphorylation, IEG induction and cardiomyocyte hypertrophy induction. Further studies will lead to the identification of the wider significance of MSK-induced pH3S28 in the hypertrophic response and how it may be manipulated for therapeutic benefit.

Materials and Methods

Reagents

Chemicals purchased were from Sigma Aldrich and molecular biology reagents were from Thermo Scientific and Life Technologies, unless stated otherwise. Tables of

antibodies and primers used in this study are included in Supplementary Tables and 3 and 4 respectively.

Animal experiments

All experiments involving animals were performed in accordance with the UK Home Office and institutional guidelines and in accordance with the European Directive 2010/63/EU and approved by the Ethical Committee for Animal Experiments of the KU Leuven (Belgium). The Msk1/2 null animals have been previously described (Arthur and Cohen, 2000; Wiggin et al., 2002b). Hypertrophic remodelling was induced in 8-10 week old male mice animals by administration of isoproterenol (Iso, Sigma-Aldrich) at 10 mg/kg/day for one week via osmotic mini-pumps (Alzet) implantation as previously described (Liu et al., 2009). Jugular vein infusion of ET-1 and Iso was performed as previously described (Archer et al., 2017) using an approved experimental protocol (license number P055/2017) approved by the Ethical Committee for Animal Experiments of the KU Leuven (Belgium), explained in detail later. Male Sprague Dawley rats subjected to six weeks of ascending aortic banding or a six-week treadmill training program were previously used to generate cardiomyocyte-specific nuclear (PCM-1 positive) RNA-sequencing data as previously described (Thienpont et al., 2017). RNA sequencing data was re-purposed for this study, focusing on the panel of IEGs. The sequencing data are available in the NCBI's Gene Expression Omnibus (GEO) database (GEO GSE66653). Animals were housed and treated according to the European Directive 2010/63/EU.

Echocardiography

Mice were anesthetised with Avertin (200 mg/kg). Cardiac function was assessed by transthoracic 2D M-mode echocardiography using an Acuson Sequoia C256 ultrasound system (Siemens) as previously described (Liu et al., 2009).

Preparation of neonatal rat ventricular myocytes (NRVMs)

Primary neonatal rat ventricular myocytes (NRVMs) were isolated from 3-4 day old male and female Wistar pups and cultured as described previously (Higazi et al., 2009). Cultures were > 95 % pure. NRVMs were seeded at a density at which they exhibited spontaneous and synchronous beating throughout the experiment. 48 h after seeding, NRVMs were washed into serum-free medium (DMEM/M199 4:1, 1 mM sodium pyruvate, 5.5 µg/mL transferrin, 5 ng/mL sodium selenite, 1 X Antibiotic-Antimycotic (Life Technologies), and 3 µM cytosine b-D-arabinofuranoside (araC) and serum-starved for 24 h. NRVMs were subsequently stimulated with the agents described. Adenoviral infections were performed by incubation with a volume of virus-containing serum-free medium sufficient to cover the cells for 4 h. Agonist treatments diluted in serum-free medium were applied 24 h post-infection with adenovirus. Endothelin-1 (ET-1, Millipore), isoproterenol hydrochloride (Iso, Sigma Aldrich) and PD184352 (PD, Sigma Aldrich) treatments were performed at a final concentration of 100 nM, 10 nM and 10 nM respectively. All cellular treatments with PD were pre-treated with PD for 30 min prior to hypertrophic agonist application (ET-1/Iso). Control cellular experiments (no treatment) were treated with the same volume of vehicle only (DMSO for ET-1 and PD).

728 **Isolation and culture of adult rat ventricular myocytes (ARVMs)**

729 Male Wistar rats (Harlan; ~200 g) were anaesthetised by CO_2 inhalation and killed by
730 cervical dislocation. ARVMs were isolated by collagenase digestion following
731 Langendorff perfusion as previously described and cultured in adult cardiomyocyte
732 medium (M199, 1 % penicillin-streptomycin-l-glutamine, 0.2 % bovine serum albumin
733 (BSA)) on laminin-coated (25 µg/ml) dishes (Drawnel et al., 2012). Adenoviral
734 infections were performed for 12 h in a minimal volume of virus-containing medium.
735 For experiments involving acute stimulation with ET-1 and Iso, cells in Tyrode were
736 plated onto laminin-coated 8 well Nunc cover glasses cells, allowed to attach for 1 h at
737 37 °C, after which the Tyrode solution was replaced with Tyrode containing DMSO
738 vehicle or Tyrode containing 10 nM PD. After 20 min, buffer was exchanged for Tyrode
739 containing 100 nM ET-1 or 10 nM Iso ± PD. After 15 min, dishes were placed on ice
740 and processed for immunostaining and imaging.

741

742 **Isolation of human ventricular cardiomyocytes**

743 Donor human tissue was collected under a study protocol approved by the ethical
744 committee of UZ Leuven (S58824), conformed to the Helsinki declaration, and was
745 con-ducted in accordance with the prevailing national and European Union regulations
746 on the use of human tissues. Donor information is displayed in Table S1.

747 Human ventricular myocytes were prepared from the explanted hearts immediately
748 after removal as previously described (Dries et al., 2018). The explants hearts were
749 collected in ice-cold modified Tyrode's solution at the time of surgery (in mM: NaCl
750 130, KCl 27, HEPES 6, $MgSO_4$ 1.2, KH_2PO_4 1.2, glucose 50; pH 7.2 with NaOH) and
751 transported to the lab. A wedge of the left ventricle with its perfusing coronary artery

was cannulated. If possible, a wedge from the left anterior descending artery was cannulated, otherwise a left circumflex branch was used. The artery and the tissue was perfused at 37 °C with a Ca^{2+}-free Tyrode's solution (in mM: NaCl 130, KCl 5.4, HEPES 6, $MgSO_4$ 1.2, KH_2PO_4 1.2, glucose 20; pH 7.2 with NaOH) for 30 min followed by enzyme perfusion for 40 min (collagenase A, Roche and protease XIV, Sigma Aldrich in Ca^{2+}-free solution) and after digestion, perfused with low Ca^{2+} Tyrode (Ca^{2+}-free solution with 0.18 mM $CaCl_2$ added). The digested tissue was minced, the suspension was filtered and the isolated myocytes were resuspended in normal Tyrode. After isolation, the cells were allowed to recover for 1 h before starting experiments or fixation. For experiments involving stimulation with Iso or ET-1, cells were plated onto poly-L-lysine coated 8 well Nunc cover glasses and allowed to attach for 1 h at 37 °C. After this period the Tyrode solution was replaced with Tyrode containing DMSO vehicle or Tyrode containing 10 nM PD. After 20 min, buffer was exchanged for Tyrode containing 100 nM ET-1 or 10 nM Iso ± PD. After 15 min, dishes were placed on ice and processed for immunostaining and imaging.

Isolation of human cardiomyocyte nuclei

Nuclei from post-mortem left ventricular tissue were isolated and flow sorted according to pericentriolar material 1 (PCM-1) staining as previously described (Bergmann and Jovinge, 2012). 500,000 nuclei were sorted into 1 ml TRIzol reagent for RNase inhibition prior to RNA isolation. Human LV samples were obtained from the KI Donatum, Karolinska Institutet, Stockholm, Sweden, with permission for the analysis of human tissue for research purposes granted by the Regional Ethics Committee in Stockholm, Sweden. Donor information from which LV cardiomyocyte nuclei were isolated is displayed in Table S2.

Histology and section preparation

Adult hearts were dissected from *Msk1/2* KO mice and covered in a layer of Tissue-Tek optimum cutting temperature (OCT) in Tissue-Tek® Cryomold® Molds (15x15x15 mm) and flash-frozen in liquid nitrogen-cooled isopentane (VWR). 10 µm ventricular sections were cut using a Leica cryostat and attached to SuperFrost Plus™ slides (VWR). Slides were frozen at -20℃ prior to immunostaining.

Sections were thawed and rehydrated in phosphate buffered saline (PBS) for 5 min, followed by 15 min fixation in 4 % paraformaldehyde (PFA). After three washes (5 min each) in PBS, sections were permeabilised for 30 min in 0.2 % Triton X-100 in PBS (PBS-TX), then washed twice with PBS. Non-specific protein binding sites were blocked by incubation in PBS-TX containing 3 % BSA or 5 % goat serum for 1 h. Primary antibodies were diluted in blocking buffer and incubated overnight at 4℃. After overnight incubation, slides were washed X3 in PBS and secondary antibodies added in blocking buffer for 1 h at room temperature. After incubation, the slides were washed and mounted in VECTASHIELD Antifade Mounting Medium containing DAPI (Vectorlabs). Confocal images were acquired using a Nikon A1R confocal microscope using a 40X 1.3 Numerical Aperture (N.A.) oil immersion objective.

Picro Sirius Red staining for fibrosis analysis

10 µm thick sections were cut from OCT embedded tissue as above. Subsequently, sections were rehydrated and stained for collagen using a Picro Sirius red staining kit (PolySciences). After staining, sections were mounted in dibutylphthalate polystyrene xylene mounting medium. Images were acquired using a Zeiss Axioplan microscope

801 configured with an Axiocam HrC camera. Polarization microscopy was performed on
802 the Sirius red stained sections to visualize collagen type I and III based on the
803 birefringence properties of collagen. The degree of fibrosis was quantified using
804 Axiovision analysis software.

805

806 **Immunofluorescence analysis**

807 Analysis of surface area of NRVM was carried out as previously described (6). Briefly,
808 NRVMs for immunofluorescence were cultured and fixed in black 96-well imaging
809 microplates (BD Biosciences). NRVMs were immunostained with primary antibodies
810 against α-Act and ANF and detected using Alexa Fluor 488 and 568-coupled
811 secondary antibodies (Table S3). After immunostaining, nuclei were labelled with
812 Hoescht (1 µg/ml in PBS for 20 min). Images were captured using a BD Pathway 855
813 high-content imaging system and Attovision software. Cell planimetry was performed
814 using ImageJ by drawing around the edge of the cells (NIH). At least 400 cells from
815 three independent experiments were analysed. These images were also used for
816 quantification of ANF protein expression as determined by counting the number of
817 NRVM exhibiting a peri-nuclear ring of ANF.

818 For confocal imaging, NRVMs were cultured in 16-well chamber slides (Nunc). Slides
819 were mounted onto a coverslip using VECTASHIELD Mounting Medium containing
820 DAPI and sealed with clear nail varnish.

821 For staining of ARVMs and human isolated cardiomyocytes, cells were fixed and
822 permeabilised in ice-cold 100 % methanol and incubated at -20 °C for 10 min. Methanol
823 was washed from the coverslips twice with PBS and further permeabilisation
824 performed by the addition of 0.5 ml ice-cold 100 % acetone and incubation at -20 °C

for 1 min. Following an additional two washes in PBS, antibody labelling was performed as described for NRVM. To further reduce background staining, blocking and secondary antibody buffers contained 1 % BSA in addition to goat serum.

Immunofluorescence analysis of cardiac sections was performed as previously described (8). Snap-frozen heart samples were embedded in OCT (VWR), cryo-sections (thickness 10 µm) were collected on SUPERFROST PLUS microscope slides (VWR), fixed in 4 % PFA in PBS for 15 min, permeabilised in 0.25 % Triton-X100 in PBS for 15 min, and blocked in 5 % Chemibloc in PBS with 0.1 % Triton-X100 (PBS-TX) for 1 h. Sections were subsequently incubated overnight at 4°C in blocking buffer with primary antibodies as per Table S3. Samples were washed extensively in PBS-TX, and incubated with Alexa Fluor® secondary antibodies (Invitrogen) at 1:500 in PBS-TX for 1 h at room temperature. Where required, DAPI was included to identify the DNA in nuclei, respectively.

Sections were mounted in VECTASHIELD with DAPI (Vector Labs) and imaged on a Nikon A1R confocal microscope through a Plan Fluor DIC H N 40x oil immersion objective (N.A.=1.3). Image stacks were collected over a 2 µm stack thickness (0.2 µm z-step). Image stacks were analysed with Volocity Image analysis software (version 6.2.1, Perkin Elmer). Cardiac myocyte nuclei were identified by PCM-1- or Nesprin-positive labelling, as previously described (Thienpont et al., 2017).

Cellular apoptosis was measured in *Msk* KO mouse cardiac sections using the TACS® 2 TdT-DAB In Situ Apoptosis Detection Kit (Bio-Techne Ltd).

Confocal images were acquired using an Olympus FV1000 point scanning microscope attached to an Olympus IX81, equipped with a 40X/1.3 NA UPlanFI oil immersion

objective or using a Nikon A1R confocal attached to a Nikon Ti microscope equipped with 40X 1.3 N.A. oil immersion objective.

Histone isolation by acid extraction

NRVMs in 6-well dishes were washed once in ice-cold PBS. 0.5 ml of fresh ice-cold PBS was added to each well, the cells scraped and placed in pre-chilled 1.5 ml tubes. Cells were pelleted by centrifugation (10 min, 300 xg, 4 °C). PBS was removed and the pellet re-suspended in 1 ml hypotonic lysis buffer. The resuspended cells were incubated on a rotator at 4 °C, 30 rpm for 30 min. At the end of this incubation, intact nuclei were pelleted by centrifugation (10 min, 10000 xg, 4 °C). Nuclei were then resuspended in 400 µl 0.2 M H2SO4 by pipetting and vortexing. Histones were acid extracted overnight at 4 °C on a rotator at 30 rpm. Following acid extraction, nuclear debris was removed by centrifugation (10 min, 16000 xg, 4 °C) and the supernatant containing isolated histones transferred to a pre-chilled tube. To precipitate proteins, 100 % trichloroacetic acid was added to the supernatant in a drop-wise manner to achieve a final concentration of 25 %. The tube was gently inverted and then incubated on ice for 6 h. At the end of this period, precipitated proteins were recovered by centrifugation (10 min, 16000 xg, 4 °C). The supernatant was aspirated and acid removed from the tube by washing the pellet in 300 µl ice-cold acetone. After centrifugation (5 min, 16000 xg, 4 °C) and removal of the supernatant, the acetone wash and spin were repeated. Finally, the supernatant was gently removed and the pellet air-dried for 20 min at room temperature. The dried pellet was resuspended in 50 µl water and incubated overnight at 4 °C on a rotator at 30 rpm to maximise protein solubilisation.

872

873 **Immunoblot analysis**

874 Cultures of NRVM were washed once in ice-cold PBS after which 80 µl pre-chilled
875 RIPA buffer was added to the dish and incubated for 5 min on ice (25 mM Tris-HCl, pH
876 7.6, 150 mM NaCl, 0.1 % SDS, 1 % NP-40, 1 % Sodium Deoxycholate supplemented
877 with 1 X Protease and Phosphatase inhibitor cocktails (Sigma Aldrich) . The cell lysate
878 was transferred to a pre-chilled tube and debris removed by centrifugation (5 min, 10
879 000 g, 4 °C). The supernatant was transferred to a clean tube and total protein
880 concentration determined using the BCA assay (Thermo Scientific). Equivalent
881 amounts of protein (10-30 µg) were loaded and samples prepared with LDS sample
882 buffer (Invitrogen, final concentration 25 %) containing 2.5 % β-mercaptoethanol and
883 boiled at 95 °C for 5 min before centrifuging briefly to remove debris.

884 Proteins were resolved on pre-cast 4-12 % NuPAGE 1.5 mm 10 well SDS gels
885 (Invitrogen). The gels were rinsed with deionised water and placed in an X-cell
886 Surelock Mini-cell running tank. The inner buffer chamber was filled with sufficient 1 X
887 MOPS SDS Running buffer (Invitrogen) to cover the wells which were then rinsed with
888 buffer expelled from a needle and syringe. 500 µl NuPAGE Antioxidant (Invitrogen)
889 was added to the inner buffer chamber. The outer buffer chamber was filled with
890 approximately 600 ml 1 X MOPS SDS Running buffer. 12 µl of Novex pre-stained sharp
891 protein markers (Invitrogen) were loaded into the first well, followed by the boiled
892 samples. Electrophoresis was performed at 200 V until the tracking dye reached the
893 end of the gel.

894 For detection of ERK or MSK, proteins were transferred to a PVDF (0.45 µm, Millipore)
895 membrane, which had been activated by immersion for 100 % methanol for 15 s and

then placed in deionised water for 2 min. For detection of histone H3, proteins were transferred to a nitrocellulose (0.2 µm, Whatman). Proteins were detected with appropriate primary antibodies and HRP-conjugated secondary antibodies (Table S3). Immunoreactive bands were detected by enhanced chemiluminescence (Pierce).

Reverse transcription quantitative PCR (RT-qPCR)

RNA was isolated from NRVMs and ARVMs using the RNeasy Micro Kit (Qiagen) and DNA removed by an on-column DNA digestion step. RNA was isolated from adult rat LV tissue, *Msk1/2* KO mouse LV tissue and human cardiomyocytes using TRIzol reagent (Invitrogen).

500-750 ng RNA was reverse transcribed using Superscript II (Invitrogen), the final cDNA synthesis reaction diluted 1/10 - 1/20 in nuclease free water and stored at -20 °C until required. Primer sequences were as previously described, unless otherwise indicated (Table S4), and were designed to span intron-exon boundaries to avoid amplification of genomic DNA (Higazi et al., 2009). The stability of a panel of reference genes was assessed using the GeNorm method for the experiments performed, and the most stable selected (Vandesompele et al., 2002). Three or four reference genes were selected for each set of experimental conditions for normalisation of gene expression qPCR analysis based on their stability for each set of samples and reaction conditions. Final primer concentration was 200 nM for all targets.

Reactions were performed on a LightCycler® 480 System (Roche) or on a CFX384 (BIO-RAD) in a 384-well format using Platinum SYBR Green qPCR SuperMix-UDG (Life Technologies). Expression analysis was carried out using the comparative ΔCt method as described (Livak and Schmittgen, 2001).

Chromatin-immunoprecipitation (ChIP)

To NRVMs in 6-well dishes in culture medium, formaldehyde was added to a concentration of 1 % and incubated for 10 min on a rocking platform at room temperature. Cross-linking was terminated by the addition of 125 mM glycine for 10 min at room temperature. After washing once in ice-cold PBS, cells were collected into 0.5 ml PBS by scraping and subsequent centrifugation (5 min, 600 xg, 4 °C). Cell pellets were re-suspended in 1 ml ice-cold hypotonic membrane lysis buffer (50 mM Tris-HCl, pH 7.5, 5 mM EDTA, 140 mM NaCl, 1 % Triton X-100, 0.5 % NP-40 supplemented with 1 X Protease and Phosphatase inhibitor cocktails). The released nuclei were pelleted by centrifugation (3 min, 12000 xg, 4 °C) and then re-suspended in 200 µl SDS lysis buffer (50 mM Tris-HCl, pH 7.5, 10 mM EDTA, 1 % SDS supplemented with 1 X Protease and Phosphatase inhibitor cocktails). Cross-linked chromatin was fragmented by sonication using a pre-chilled Diagenode Bioruptor on the high power setting for three x 5 min cycles of 30 s ‘on’, 30 s ‘off’. The sonication protocol produced fragments predominantly below 500 bp. Wash buffer + (10 mM Tris-HCl, pH 7.5, 140 mM NaCl, 1 mM EDTA, 0.5 mM EGTA, 1 % Triton X-100, 0.1 % SDS and 0.1% Na deoxycholate supplemented with 1 X Protease and Phosphatase inhibitor cocktails) was then added to the lysate. After removal of remaining debris by centrifugation (10 min, 12000 xg, 4 °C), the supernatant (sonicated chromatin) was processed for immunoprecipitation.

Proteins of interest were precipitated using antibodies pre-conjugated to Dynabeads Protein A (Invitrogen). To this end, beads were washed in 4 changes of wash buffer and collected by the use of a DynaMag Magnet. Per ChIP, 10 µl washed beads and 5 µg Brg1 or phosphorylated H3S28 antibody were added to 90 µl wash buffer and

incubated for two h at 40 rpm on a rotator at 4 °C. For the negative control ChIP, beads were used in the absence of specific antibody.

Prior to IP, wash buffer was removed from pre-prepared antibody-bead complexes and 200 µl chromatin added to each tube. 200 µl chromatin was reserved from each experimental condition as an Input sample. Chromatin was incubated with the antibody-bead complexes overnight at 4 °C on a 40 rpm rotator after which unbound chromatin was washed from the beads. Wash buffer was used for the first two washes, followed by one wash in high-salt wash buffer (wash buffer + with 500 mM NaCl) and finally two washes in TE buffer. At the end of the washes, the solution was transferred to a fresh tube and TE buffer removed from the beads. Elution of chromatin from the beads and protein digest with proteinase K were combined into one step. To this end, 150 µl complete elution buffer (20 mM Tris-HCl, pH 7.5, 50 mM NaCl, 5 mM EDTA, 1% SDS and 100 µg/ml proteinase K (Sigma)) was added and the beads incubated for 4 h at 68 °C with shaking at 1300 rpm. The supernatant was removed from the tube and 150 µl elution buffer (complete elution buffer without SDS and Proteinase K) added. After a further 5 min incubation at 68 °C, the two supernatants were combined. Input samples were processed in parallel with the ChIP samples. DNA was purified from each supernatant using the QIAEX II Gel extraction kit (Qiagen) following the manufacturer's protocol for concentrating DNA from solutions. DNA was eluted in 40 µl buffer EB and stored at -20 °C until required.

Precipitated DNA for each experimental condition and antibody was quantified by qPCR using SYBR-GreenER in 12.5 µl reactions performed in triplicate (Invitrogen). Primers were designed to amplify the promoter sequences of c-Fos and c-Jun and the sequences of the primers used are given in appendix A. Primer binding sites were selected that encompassed predicted transcription factor binding sites. qPCR was

970 performed using a CFX96 (BIO-RAD) or Roche Light Cycler480 real-time PCR
971 instrument and cycling parameters were taken from the manufacturer's instructions for
972 SYBR-GreenER (Thermo Life Technologies).

973 The Ct values from triplicate technical replicates from each sample were averaged to
974 generate SampleCT and InputCt values. The values were analysed by expressing
975 enrichment of the immunoprecipitated DNA for each antibody as a percentage of the
976 input sample for the relevant experimental condition according to the equation,
977 Enrichment = 2(Sample Ct – Input Ct). ChIPs were repeated on at least 4 independent
978 experimental samples.

979

980 **Wistar rat jugular vein infusion of endothelin-1/isoproterenol**

981 Experimental protocols were approved by the local ethical committee (Ethische
982 Commissie, Dierproeven, KU Leuven), under license number P055/2017. 250-300 g
983 Wistar (RccHan:WIST) male rats were obtained from Harlan (NL). Anesthesia was
984 induced using ketamine and xylazine in combination (100 mg/kg ketamine, 10 mg/kg
985 xylazine) by IP. Body temperature was maintained throughout the procedure with a
986 heated mat (Sanitas).

987 A small area of chest was shaved with depilatory cream (Veet) and limbs secured with
988 tape. A small incision was made just above and to the right hand side of the sternum
989 and the skin stretched thin with a hemostat to make the jugular vein visible. A 30 gauge
990 needle attached to a cannula (2F x 30 cm, green, Portex) was inserted into the jugular
991 vein, just before it branches and the vein disappears under the pectoral muscle.

992 The cannula was attached to a 5 ml syringe and a dispensing pump (Harvard
993 Apparatus) dispensing the required volume (300-500 µl) over a 15-min period. A slow

steady release of the dosage in this manner was required to reduce the acute vasoconstrictive effect of a single rapid injection of the same dosage.

Endothelin-1 (Millipore) was administered at a final dosage of 1000 ng/kg and isoproterenol hydrochloride (Sigma Aldrich) at 50 µg/kg. Final working concentrations prepared in sterile saline and vehicle-only controls (Ctrl) were administered the same volume of sterile saline over a 15 min period. On withdrawal of the needle, medical gauze was placed over the wound and pressure applied until bleeding stopped. The wound was cleaned with iodine solution and for the 24 h time point, the skin was sutured together with interrupted stiches.

For the 15 min time point, rats were sacrificed by cervical dislocation and heart removed for dissection immediately. For the 24 h time point, rats were allowed to recover alone in a cage on heated mat, with easy access to food and water. The humane 24 h end-point was performed by anesthesia induction in an isoflurane chamber followed by cervical dislocation and immediate removal of the heart.

Whole hearts were removed and placed in ice cold PBS briefly to remove excess blood, dissected using a sterile surgical scalpel in PBS on ice and weighed on a microbalance before snap-freezing in liquid nitrogen and stored at -80 °C.

Adenoviral methods

Adenoviruses were produced and amplified in HEK293 cells and purified as previously described (Archer et al., 2017). Adenoviruses to express the WT and catalytically dead D565A mutant (DN) of MSK1 were generated using the AdEasy method by sub-cloning

the cDNA for MSK1 or its mutant from a pCMV5 backbone (kindly provided by Prof D Alessi, University of Dundee) into pShuttle CMV (Alessi, 1997). PacI digested recombinant plasmids were transfected into HEK293 cells and crude adenovirus harvested after 10-14 days. Adenoviruses for dominant negative (DN)-Jun and AP-1 luciferase were purchased from Vector Biolabs. All viruses were amplified in HEK293 cells, purified using the Vivapure Adenopack 100 (Sartorius) and titrated by end-point dilution in HEK293 cells.

Analysis of luciferase reporter activity

The AP-1 luciferase reporter was expressed using an adenoviral vector and luciferase activity determined using a luciferase assay kit from Promega as previously described (Higazi et al., 2009). Briefly, cultures of NRVM in 48 well plates were infected in duplicate and agonist treatments applied for 24 h. After removal of medium, cells were lysed in 150 µl 1X cell culture lysis buffer (Promega). Luciferase activity present in 10 µl of lysate clarified by centrifugation was then quantitated in white 96-well luminometer plate (Microlumat Plus 1b 96V instrument, Berthold Technologies) using 50 µl of luciferase assay reagent (Promega).

Small interfering RNA (siRNA) knockdown

Stealth™ siRNAs were purchased from Invitrogen. To achieve sufficient knockdown of *Msk1* or *Brg1*, two siRNAs targeting different regions of the target mRNA were selected. Medium GC-content non-silencing siRNA (Invitrogen) was transfected as a negative control. Transfections were performed at the onset of the serum starvation period using Dharmafect I and Accell medium (Dharmacon). To transfect NRVM

cultured in 12-well dishes, 200 pmol siRNA duplexes were made up to 100 µl total volume in Accell media and the solution mixed by pipetting. In a separate tube, 6 µl Dharmafect I was added to 94 µl Accell medium and mixed. After incubation for 5 min at room temperature, the tubes were combined, mixed and incubated for a further 20 min at room temperature. During this incubation, NRVM culture medium was replaced with 800 µl pre-warmed Accell medium. At the end of the 20 min incubation, transfection complexes were added to the cultures in a drop-wise manner and incubated with the cells for 6 h. Post-transfection, Accell medium was replaced with fresh maintenance medium and the remainder of the serum starvation period carried out.

Statistical analysis

Data were collated in Microsoft Excel and statistical analysis performed using GraphPad Prism v7.0 or v8.0. Data is presented as the mean of at least three independent experiments ± the standard error of the mean (SEM). The number of independent experiments for each figure is indicated in the figure legend. For comparison between two groups, p-values were calculated using the unpaired two-tailed t-test. For comparison of two groups where normalisation of data had been performed (i.e. one value was fixed at 1.0) a two-tailed paired t-test was used. To calculate p-values for data comparing three or more groups, one-way ANOVA with Bonferroni's multiple comparison test for p value correction. P-values less than 0.05 were taken as significant. Individual (adjusted) p values are indicated on the figures.

References

Alessi, D.R. (1997). The protein kinase C inhibitors Ro 318220 and GF 109203X are equally potent inhibitors of MAPKAP kinase-1beta (Rsk-2) and p70 S6 kinase. FEBS Lett. *402*, 121–123.

Alkass, K., Panula, J., Westman, M., Wu, T.-D., Guerquin-Kern, J.-L., and Bergmann, O. (2015). No Evidence for Cardiomyocyte Number Expansion in Preadolescent Mice. Cell *163*, 1026–1036.

Archer, C.R., Robinson, E.L., Drawnel, F.M., and Roderick, H.L. (2017). Endothelin-1 promotes hypertrophic remodelling of cardiac myocytes by activating sustained signalling and transcription downstream of endothelin type A receptors. Cell. Signal. *36*, 240–254.

Arthur, J.S., and Cohen, P. (2000). MSK1 is required for CREB phosphorylation in response to mitogens in mouse embryonic stem cells. FEBS Lett. *482*, 44–48.

Auger-Messier, M., Accornero, F., Goonasekera, S.A., Bueno, O.F., Lorenz, J.N., van Berlo, J.H., Willette, R.N., and Molkentin, J.D. (2013). Unrestrained p38 MAPK Activation in Dusp1/4 Double Null Mice Induces Cardiomyopathy. Circ Res *112*, 48–56.

Awad, S., Kunhi, M., Little, G.H., Bai, Y., An, W., Bers, D., Kedes, L., and Poizat, C. (2013). Nuclear CaMKII enhances histone H3 phosphorylation and remodels chromatin during cardiac hypertrophy. Nucleic Acids Res. *41*, 7656–7672.

Awad, S., Al-Haffar, K.M.A., Marashly, Q., Quijada, P., Kunhi, M., Al-Yacoub, N., Wade, F.S., Mohammed, S.F., Al-Dayel, F., Sutherland, G., et al. (2015). Control of histone H3 phosphorylation by CaMKIIδ in response to haemodynamic cardiac stress. J. Pathol. *235*, 606–618.

Backs, J., Song, K., Bezprozvannaya, S., Chang, S., and Olson, E.N. (2006). CaM kinase II selectively signals to histone deacetylase 4 during cardiomyocyte hypertrophy. J Clin Invest *116*, 1853–1864.

Bain, J., Plater, L., Elliott, M., Shpiro, N., Hastie, C.J., Mclauchlan, H., Klevernic, I., Arthur, J.S.C., Alessi, D.R., and Cohen, P. (2007). The selectivity of protein kinase inhibitors: a further update. Biochem J *408*, 297–315.

Balmanno, K., and Cook, S.J. (1999). Sustained MAP kinase activation is required for the expression of cyclin D1, p21Cip1 and a subset of AP-1 proteins in CCL39 cells. Oncogene *18*, 3085–3097.

Bergmann, O., and Jovinge, S. (2012). Isolation of Cardiomyocyte Nuclei from Post-mortem Tissue. J Vis Exp.

Beyer, M.E., Nerz, S., Krämer, B.K., and Hoffmeister, H.M. (1994). Hemodynamic and inotropic effects of endothelin-1 in vivo. Basic Res. Cardiol. *89*, 39–49.

1102 Boluyt, M.O., Long, X., Eschenhagen, T., Mende, U., Schmitz, W., Crow, M.T., and
1103 Lakatta, E.G. (1995). Isoproterenol infusion induces alterations in expression of
1104 hypertrophy-associated genes in rat heart. Am. J. Physiol. *269*, H638-647.

1105 Bueno, O.F., De Windt, L.J., Tymitz, K.M., Witt, S.A., Kimball, T.R., Klevitsky, R.,
1106 Hewett, T.E., Jones, S.P., Lefer, D.J., Peng, C.-F., et al. (2000). The MEK1–ERK1/2
1107 signaling pathway promotes compensated cardiac hypertrophy in transgenic mice.
1108 EMBO J *19*, 6341–6350.

1109 Chen, L., Glover, J.N., Hogan, P.G., Rao, A., and Harrison, S.C. (1998). Structure of
1110 the DNA-binding domains from NFAT, Fos and Jun bound specifically to DNA. Nature
1111 *392*, 42–48.

1112 Chiu, R., Boyle, W.J., Meek, J., Smeal, T., Hunter, T., and Karin, M. (1988). The c-Fos
1113 protein interacts with c-Jun/AP-1 to stimulate transcription of AP-1 responsive genes.
1114 Cell *54*, 541–552.

1115 Clayton, A.L., and Mahadevan, L.C. (2003). MAP kinase-mediated phosphoacetylation
1116 of histone H3 and inducible gene regulation. FEBS Lett. *546*, 51–58.

1117 Clayton, A.L., Rose, S., Barratt, M.J., and Mahadevan, L.C. (2000).
1118 Phosphoacetylation of histone H3 on c-fos- and c-jun-associated nucleosomes upon
1119 gene activation. EMBO J *19*, 3714–3726.

1120 Deak, M., Clifton, A.D., Lucocq, J.M., and Alessi, D.R. (1998a). Mitogen- and stress-
1121 activated protein kinase-1 (MSK1) is directly activated by MAPK and SAPK2/p38, and
1122 may mediate activation of CREB. The EMBO Journal *17*, 4426–4441.

1123 Deak, M., Clifton, A.D., Lucocq, L.M., and Alessi, D.R. (1998b). Mitogen- and stress-
1124 activated protein kinase-1 (MSK1) is directly activated by MAPK and SAPK2/p38, and
1125 may mediate activation of CREB. EMBO J. *17*, 4426–4441.

1126 Drawnel, F.M., Wachten, D., Molkentin, J.D., Maillet, M., Aronsen, J.M., Swift, F.,
1127 Sjaastad, I., Liu, N., Catalucci, D., Mikoshiba, K., et al. (2012). Mutual antagonism
1128 between IP3RII and miRNA-133a regulates calcium signals and cardiac hypertrophy.
1129 J Cell Biol *199*, 783–798.

1130 Dries, E., Santiago, D.J., Gilbert, G., Lenaerts, I., Vandenberk, B., Nagaraju, C.K.,
1131 Johnson, D.M., Holemans, P., Roderick, H.L., Macquaide, N., et al. (2018).
1132 Hyperactive ryanodine receptors in human heart failure and ischaemic cardiomyopathy
1133 reside outside of couplons. Cardiovasc. Res. *114*, 1512–1524.

1134 Duncan, E.A., Anest, V., Cogswell, P., and Baldwin, A.S. (2006). The kinases MSK1
1135 and MSK2 are required for epidermal growth factor-induced, but not tumor necrosis
1136 factor-induced, histone H3 Ser10 phosphorylation. J. Biol. Chem. *281*, 12521–12525.

1137 Dyson, M.H., Thomson, S., Inagaki, M., Goto, H., Arthur, S.J., Nightingale, K., Iborra,
1138 F.J., and Mahadevan, L.C. (2005). MAP kinase-mediated phosphorylation of distinct
1139 pools of histone H3 at S10 or S28 via mitogen- and stress-activated kinase 1/2. Journal
1140 of Cell Science *118*, 2247–2259.

Eferl, R., and Wagner, E.F. (2003). AP-1: a double-edged sword in tumorigenesis. Nat. Rev. Cancer *3*, 859–868.

Garrington, T.P., and Johnson, G.L. (1999). Organization and regulation of mitogen-activated protein kinase signaling pathways. Curr. Opin. Cell Biol. *11*, 211–218.

Gehani, S.S., Agrawal-Singh, S., Dietrich, N., Christophersen, N.S., Helin, K., and Hansen, K. (2010). Polycomb group protein displacement and gene activation through MSK-dependent H3K27me3S28 phosphorylation. Mol. Cell *39*, 886–900.

Gille, H., Sharrocks, A.D., and Shaw, P.E. (1992). Phosphorylation of transcription factor p62 TCF by MAP kinase stimulates ternary complex formation at c- fos promoter. Nature *358*, 414–417.

Gilsbach, R., Preissl, S., Grüning, B.A., Schnick, T., Burger, L., Benes, V., Würch, A., Bönisch, U., Günther, S., Backofen, R., et al. (2014). Dynamic DNA methylation orchestrates cardiomyocyte development, maturation and disease. Nature Communications *5*, 1–13.

Glover, J.N., and Harrison, S.C. (1995). Crystal structure of the heterodimeric bZIP transcription factor c-Fos-c-Jun bound to DNA. Nature *373*, 257–261.

Hang, C.T., Yang, J., Han, P., Cheng, H.-L., Shang, C., Ashley, E., Zhou, B., and Chang, C.-P. (2010). Chromatin regulation by Brg1 underlies heart muscle development and disease. Nature *466*, 62–67.

Heineke, J., and Molkentin, J.D. (2006). Regulation of cardiac hypertrophy by intracellular signalling pathways. Nature Reviews Molecular Cell Biology *7*, 589–600.

Hess, J., Angel, P., and Schorpp-Kistner, M. (2004). AP-1 subunits: quarrel and harmony among siblings. J. Cell. Sci. *117*, 5965–5973.

Higazi, D.R., Fearnley, C.J., Drawnel, F.M., Talasila, A., Corps, E.M., Ritter, O., McDonald, F., Mikoshiba, K., Bootman, M.D., and Roderick, H.L. (2009). Endothelin-1-stimulated InsP3-induced Ca2+ release is a nexus for hypertrophic signaling in cardiac myocytes. Mol. Cell *33*, 472–482.

Hilfiker-Kleiner, D., Hilfiker, A., Castellazzi, M., Wollert, K.C., Trautwein, C., Schunkert, H., and Drexler, H. (2006). JunD attenuates phenylephrine-mediated cardiomyocyte hypertrophy by negatively regulating AP-1 transcriptional activity. Cardiovasc Res *71*, 108–117.

Iwaki, K., Sukhatme, V.P., Shubeita, H.E., and Chien, K.R. (1990). Alpha- and beta-adrenergic stimulation induces distinct patterns of immediate early gene expression in neonatal rat myocardial cells. fos/jun expression is associated with sarcomere assembly; Egr-1 induction is primarily an alpha 1-mediated response. J. Biol. Chem. *265*, 13809–13817.

Izumo, S., Nadal-Ginard, B., and Mahdavi, V. (1988). Protooncogene induction and reprogramming of cardiac gene expression produced by pressure overload. Proc. Natl. Acad. Sci. U.S.A. *85*, 339–343.

1180 Johannessen, M., Delghandi, M.P., and Moens, U. (2004). What turns CREB on? Cell.
1181 Signal. *16*, 1211–1227.

1182 Karin, M., Liu, Z., and Zandi, E. (1997). AP-1 function and regulation. Current Opinion
1183 in Cell Biology *9*, 240–246.

1184 Kasper, L.H., Thomas, M.C., Zambetti, G.P., and Brindle, P.K. (2011). Double null cells
1185 reveal that CBP and p300 are dispensable for p53 targets p21 and Mdm2 but variably
1186 required for target genes of other signaling pathways. Cell Cycle *10*, 212–221.

1187 Kim, J.-Y., Kim, K.-B., Son, H.-J., Chae, Y.-C., Oh, S.-T., Kim, D.-W., Pak, J.H., and
1188 Seo, S.-B. (2012). H3K27 methylation and H3S28 phosphorylation-dependent
1189 transcriptional regulation by INHAT subunit SET/TAF-Iβ. FEBS Letters *586*, 3159–
1190 3165.

1191 Kim-Mitsuyama, S., Izumi, Y., Izumiya, Y., Namba, M., Yoshida, K., Wake, R.,
1192 Yoshiyama, M., and Iwao, H. (2006). Dominant-negative c-Jun inhibits rat cardiac
1193 hypertrophy induced by angiotensin II and hypertension. Gene Therapy *13*, 348–355.

1194 Liao, P., Georgakopoulos, D., Kovacs, A., Zheng, M., Lerner, D., Pu, H., Saffitz, J.,
1195 Chien, K., Xiao, R.-P., Kass, D.A., et al. (2001). The in vivo role of p38 MAP kinases
1196 in cardiac remodeling and restrictive cardiomyopathy. Proc Natl Acad Sci U S A *98*,
1197 12283–12288.

1198 Liu, R., van Berlo, J.H., York, A.J., Maillet, M., Vagnozzi, R.J., and Molkentin, J.D.
1199 (2016). DUSP8 Regulates Cardiac Ventricular Remodeling by Altering ERK1/2
1200 Signaling. Circ Res *119*, 249–260.

1201 Liu, W., Zi, M., Jin, J., Prehar, S., Oceandy, D., Kimura, T.E., Lei, M., Neyses, L.,
1202 Weston, A.H., Cartwright, E.J., et al. (2009). Cardiac-specific deletion of mkk4 reveals
1203 its role in pathological hypertrophic remodeling but not in physiological cardiac growth.
1204 Circ. Res. *104*, 905–914.

1205 Livak, K.J., and Schmittgen, T.D. (2001). Analysis of relative gene expression data
1206 using real-time quantitative PCR and the 2(-Delta Delta C(T)) Method. Methods *25*,
1207 402–408.

1208 Malakhova, M., Kurinov, I., Liu, K., Zheng, D., D'Angelo, I., Shim, J.-H., Steinman, V.,
1209 Bode, A.M., and Dong, Z. (2009). Structural Diversity of the Active N-Terminal Kinase
1210 Domain of p90 Ribosomal S6 Kinase 2. PLOS ONE *4*, e8044.

1211 Markou, T., and Lazou, A. (2002). Phosphorylation and activation of mitogen- and
1212 stress-activated protein kinase-1 in adult rat cardiac myocytes by G-protein-coupled
1213 receptor agonists requires both extracellular-signal-regulated kinase and p38 mitogen-
1214 activated protein kinase. Biochem. J. *365*, 757–763.

1215 Markou, T., Hadzopoulou-Cladaras, M., and Lazou, A. (2004). Phenylephrine induces
1216 activation of CREB in adult rat cardiac myocytes through MSK1 and PKA signaling
1217 pathways. J. Mol. Cell. Cardiol. *37*, 1001–1011.

Markou, T., Cieslak, D., Gaitanaki, C., and Lazou, A. (2009). Differential roles of MAPKs and MSK1 signalling pathways in the regulation of c-Jun during phenylephrine-induced cardiac myocyte hypertrophy. Mol. Cell. Biochem. *322*, 103–112.

McCoy, C.E., Campbell, D.G., Deak, M., Bloomberg, G.B., and Arthur, J.S.C. (2005). MSK1 activity is controlled by multiple phosphorylation sites. Biochem. J. *387*, 507–517.

Mutlak, M., and Kehat, I. (2015). Extracellular signal-regulated kinases 1/2 as regulators of cardiac hypertrophy. Front Pharmacol *6*.

Petrich, B.G., Molkentin, J.D., and Wang, Y. (2003). Temporal activation of c-Jun N-terminal kinase in adult transgenic heart via cre-loxP-mediated DNA recombination. FASEB J. *17*, 749–751.

Phair, R.D., and Misteli, T. (2000). High mobility of proteins in the mammalian cell nucleus. Nature *404*, 604–609.

Purcell, N.H., Wilkins, B.J., York, A., Saba-El-Leil, M.K., Meloche, S., Robbins, J., and Molkentin, J.D. (2007). Genetic inhibition of cardiac ERK1/2 promotes stress-induced apoptosis and heart failure but has no effect on hypertrophy in vivo. Proc. Natl. Acad. Sci. U.S.A. *104*, 14074–14079.

Roux, P.P., and Blenis, J. (2004). ERK and p38 MAPK-activated protein kinases: a family of protein kinases with diverse biological functions. Microbiol. Mol. Biol. Rev. *68*, 320–344.

Saadatmand, A.R., Sramek, V., Weber, S., Finke, D., Dewenter, M., Sticht, C., Gretz, N., Wüstemann, T., Hagenmueller, M., Kuenzel, S.R., et al. (2019). CaM kinase II regulates cardiac hemoglobin expression through histone phosphorylation upon sympathetic activation. PNAS *116*, 22282–22287.

Sanna, B., Bueno, O.F., Dai, Y.-S., Wilkins, B.J., and Molkentin, J.D. (2005). Direct and Indirect Interactions between Calcineurin-NFAT and MEK1-Extracellular Signal-Regulated Kinase 1/2 Signaling Pathways Regulate Cardiac Gene Expression and Cellular Growth. Mol Cell Biol *25*, 865–878.

Savarese, G., and Lund, L.H. (2017). Global Public Health Burden of Heart Failure. Card Fail Rev *3*, 7–11.

Selvetella, G., Hirsch, E., Notte, A., Tarone, G., and Lembo, G. (2004). Adaptive and maladaptive hypertrophic pathways: points of convergence and divergence. Cardiovasc Res *63*, 373–380.

Soloaga, A., Thomson, S., Wiggin, G.R., Rampersaud, N., Dyson, M.H., Hazzalin, C.A., Mahadevan, L.C., and Arthur, J.S.C. (2003a). MSK2 and MSK1 mediate the mitogen- and stress-induced phosphorylation of histone H3 and HMG-14. EMBO J *22*, 2788–2797.

Soloaga, A., Thomson, S., Wiggin, G.R., Rampersaud, N., Dyson, M.H., Hazzalin, C.A., Mahadevan, L.C., and Arthur, J.S.C. (2003b). MSK2 and MSK1 mediate the

mitogen- and stress-induced phosphorylation of histone H3 and HMG-14. EMBO J *22*, 2788–2797.

Song, H.K., Hong, S.-E., Kim, T., and Kim, D.H. (2012). Deep RNA Sequencing Reveals Novel Cardiac Transcriptomic Signatures for Physiological and Pathological Hypertrophy. PLoS One *7*.

Tachibana, H., Perrino, C., Takaoka, H., Davis, R.J., Naga Prasad, S.V., and Rockman, H.A. (2006). JNK1 is required to preserve cardiac function in the early response to pressure overload. Biochem. Biophys. Res. Commun. *343*, 1060–1066.

Takeuchi, K., Yoshikawa, J., Omura, T., Yoshiyama, M., Yoshida, K., Nakamura, Y., Kim, S., Omura, T., Yoshiyama, M., Yoshida, K., et al. Dominant Negative Mutant of c-Jun Inhibits Cardiomyocyte Hypertrophy Induced by Endothelin 1 and Phenylephrine.

Thienpont, B., Aronsen, J.M., Robinson, E.L., Okkenhaug, H., Loche, E., Ferrini, A., Brien, P., Alkass, K., Tomasso, A., Agrawal, A., et al. (2017). The H3K9 dimethyltransferases EHMT1/2 protect against pathological cardiac hypertrophy. J Clin Invest *127*, 335–348.

Torgerson, T.R., Colosia, A.D., Donahue, J.P., Lin, Y.Z., and Hawiger, J. (1998). Regulation of NF-kappa B, AP-1, NFAT, and STAT1 nuclear import in T lymphocytes by noninvasive delivery of peptide carrying the nuclear localization sequence of NF-kappa B p50. J. Immunol. *161*, 6084–6092.

Ulm, S., Liu, W., Zi, M., Tsui, H., Chowdhury, S.K., Endo, S., Satoh, Y., Prehar, S., Wang, R., Cartwright, E.J., et al. (2014). Targeted deletion of ERK2 in cardiomyocytes attenuates hypertrophic response but provokes pathological stress induced cardiac dysfunction. Journal of Molecular and Cellular Cardiology *72*, 104–116.

Vandesompele, J., De Preter, K., Pattyn, F., Poppe, B., Van Roy, N., De Paepe, A., and Speleman, F. (2002). Accurate normalization of real-time quantitative RT-PCR data by geometric averaging of multiple internal control genes. Genome Biology *3*, research0034.1.

Watson, P.A., Birdsey, N., Huggins, G.S., Svensson, E., Heppe, D., and Knaub, L. (2010). Cardiac-specific overexpression of dominant-negative CREB leads to increased mortality and mitochondrial dysfunction in female mice. Am. J. Physiol. Heart Circ. Physiol. *299*, H2056-2068.

Wiggin, G.R., Soloaga, A., Foster, J.M., Murray-Tait, V., Cohen, P., and Arthur, J.S.C. (2002a). MSK1 and MSK2 are required for the mitogen- and stress-induced phosphorylation of CREB and ATF1 in fibroblasts. Mol. Cell. Biol. *22*, 2871–2881.

Wiggin, G.R., Soloaga, A., Foster, J.M., Murray-Tait, V., Cohen, P., and Arthur, J.S.C. (2002b). MSK1 and MSK2 Are Required for the Mitogen- and Stress-Induced Phosphorylation of CREB and ATF1 in Fibroblasts. Mol Cell Biol *22*, 2871–2881.

Windak, R., Müller, J., Felley, A., Akhmedov, A., Wagner, E.F., Pedrazzini, T., Sumara, G., and Ricci, R. (2013). The AP-1 Transcription Factor c-Jun Prevents Stress-Imposed Maladaptive Remodeling of the Heart. PLoS One *8*.

Wu Guangyu, Yussman Martin G., Barrett Thomas J., Hahn Harvey S., Osinska Hanna, Hilliard George M., Wang Xuejun, Toyokawa Tsuyoshi, Yatani Atsuko, Lynch Roy A., et al. (2001). Increased Myocardial Rab GTPase Expression. Circulation Research *89*, 1130–1137.

Yang, C.-M., Luo, S.-F., Hsieh, H.-L., Chi, P.-L., Lin, C.-C., Wu, C.-C., and Hsiao, L.-D. (2010). Interleukin-1beta induces ICAM-1 expression enhancing leukocyte adhesion in human rheumatoid arthritis synovial fibroblasts: involvement of ERK, JNK, AP-1, and NF-kappaB. J. Cell. Physiol. *224*, 516–526.

Zhong, S., Jansen, C., She, Q.-B., Goto, H., Inagaki, M., Bode, A.M., Ma, W.-Y., and Dong, Z. (2001). Ultraviolet B-induced Phosphorylation of Histone H3 at Serine 28 Is Mediated by MSK1. J. Biol. Chem. *276*, 33213–33219.

Acknowledgments

We would like to thank Dario Alessi (FRS FRSE FMedSci, University of Dundee) for providing the pCMV5 backbone vector for sub-cloning of MSK1 and Peter Pokreisz (CoBioRes NV and KU Leuven) for assistance in establishing techniques for jugular vein infusion of rats.

Funding

This work was supported by an Odysseus Award from the Research Foundation Flanders (Fonds Wetenschappelijk Onderzoek; FWO, 90663), the Babraham Institute, the Biotechnology and Biological Sciences Research Council (BBSRC, BBS/E/B/0000C116, BBS/E/B/000C0402) and The Royal Society (University Research Fellowship to H.L.R., UF041311). F.M.D. and C.R.A. were supported by studentships from the BBSRC (BBS/E/B/0000L715 and BBS/E/B/0000L726 respectively). E.L.R. was funded through a Wellcome Trust PhD fellowship (Cardiovascular & Disease) and an International scholarship from the KU Leuven Faculty of Medicine. SM received a Research Grant from the FWO (1524317N).

Author contributions:

Conceptualisation Ideas; E.L.R., F.D., S.M., H.L.R.

Data curation and Formal analysis; E.L.R., F.D., S.M., C.R.A., W.L., H.O., K.A., J.M.A., C.K.N., S.C.A., H.L.R.

Investigation; E.L.R., F.D., S.M., C.A., H.O., K.A., J.M.A., C.K.N., W.L., H.L.R.

Writing - Original Draft Preparation; E.L.R., F.D., H.L.R.

Writing - Review & Editing; all authors

Resource provision; O.B., K.A., J.M.A., I.S., K.R.S.

Supervision Oversight and Leadership; S.C.A., I.S., K.R.S., O.B., H.L.R.

Competing interests

No conflict of interest to declare.

Figure Legends

Figure 1: Pharmacological and molecular suppression of ERK signalling attenuates IEG induction and hypertrophy in vitro

A. RT-qPCR gene expression analysis for *Nppa/Anf* mRNA in NRVMs +/- 30 min pre-treatment with PD184352 (PD) +/- 15 min ET-1. N=7. **B.** Cell area (μm^2) as a measure of cardiomyocyte hypertrophy in NRVMs +/- PD +/- ET-1. N=4. **C.** Immunostaining for Anf (red), sarcomeric alpha-actinin (α-Act) (green) and nuclear stained with DAPI (blue) in NRVMs +/- PD +/- ET-1. Quantification (left) represents individual mean data

points for N=4, representative images (right). The scale bar represents 25 µm. **D.** RT-qPCR analysis of immediate early genes (IEGs) *c-Jun* and *c-Fos* mRNA expression in NRVMs +/- PD +/- ET-1. N=3. **E.** AP-1 luciferase assay as a readout of AP-1 transcriptional activity in NRVMs +/- PD +/- ET-1 relative to untreated. N=3. **F.** Cell area (μm^2) measurements for NRVMs infected with either control or DN-Jun (dominant negative, kinase dead) adenoviral vectors +/- ET-1. Individual data points are represented by N=4. **G.** RT-qPCR analysis of *Nppa*/Anf mRNA expression in NRVMs +/- DN-Jun +/- ET-1, N=4.

Figure S1: IEG induction is activated by acute hypertrophic stimulation and attenuated by suppression of ERK signalling in vitro

A. RT-qPCR analysis of *Nppb/Bnp* mRNA expression in NRVMs 24 h after ET-1 exposure. N=6. **B.** RT-qPCR gene expression analysis of *JunD, FosL* and *FosB* mRNA in NRVMs +/- ET-1 treatment for 15 min. N=6. **C.** Schematic diagram of the kinase signalling cascade induced by ET-1 stimulation resulting in ERK1/2 activation. Pharmacological inhibition of MEK1 by PD184352 (PD) is indicated. **D.** Immunoblot analysis for phosphorylated ERK in NRVMs +/- PD +/- ET-1. Left: Representative immunoblot for phosphorylated ERK (pERK), normalised to total ERK (T-ERK) and sarcomeric α-Act. Right: Quantitation of relative p-ERK normalised to T-ERK and α-Act. N=5.

Figure 2: Neurohumoral signalling-induced ERK1/2 activation results in histone H3S28 phosphorylation at IEG promoter regions

A. Immunoblot analysis of pH3S10 and pH3S28. Left: Representative immunoblots from 1 NRVM preparation probing for pH3S10 and pH3S28 in acid extracted histones from NRVMs exposed to ET-1 for 0, 10 and 30 min in the presence or absence of PD. Right: Levels of phosphorylated histone normalised to total H3 are shown. N=6. **B.** Confocal immunofluorescence analysis of pH3S28 in cardiomyocytes in ventricular cardiac sections prepared from rats infused with ET-1 or Iso for 15 min. Cardiomyocyte nuclei were demarcated by pericentriolar material 1 (Pcm-1; in green) perinuclear staining. Nuclei are stained with DAPI (blue) and pH3S28 in magenta. Scale bar = 25 µm. The plot (left) shows quantification of nuclear pH3S28 in Pcm-1 positive nuclei. N=4. **C.** RT-qPCR gene expression analysis of IEGs *c-Jun* and *c-Fos* mRNA in left ventricular tissue from Wistar rats administered with ET-1 or Iso through jugular vein infusion and sacrificed 15 min later. N=7. **D.** Chromatin immunoprecipitation-qPCR (ChIP-qPCR) analysis of pH3S28 at IEG promoters, *c-Jun* and *c-Fos* in adult male Wistar rats that were administered ET-1 or Iso through jugular vein infusion and sacrificed 15 min later. Top: schematic for the site of ChIP primer amplification relative to the transcription start sites. Below: quantification of enrichment compared with control (untreated) rats. N=3.

Figure S2: H3 Ser28 phosphorylation is associated with IEG induction and cardiac hypertrophy

A. RT-qPCR analysis of immediate early genes *JunD, FosL1, FosB* and of *Smarca4 (Brg1*) mRNA in hearts from adult male Wistar rats that were administered ET-1 or Iso through jugular vein administration and sacrificed 15 min later. N7 C, N=8 ET-1, N=6 Iso. **B.** RT-qPCR expression analysis for cardiac hypertrophy-associated foetal genes *Nppa*/*Anf* and *Nppb*/*Bnp* mRNA in adult male Wistar rats that were administered ET-1

or Iso through jugular vein administration and sacrificed 15 min later. N= 7 C, N=8 ET-1, N=6 Iso.

Figure 3: Activated MSK is required for H3 Ser28 phosphorylation and Brg-1-driven IEG induction in cardiomyocytes

A. Immunoblot showing levels of phosphorylated (activated) MSK in NRVMs +/- PD +/- ET-1, normalised to αAct as a loading control. Left: Representative immunoblot. Right: Quantification of pMSK relative to control vehicle treated cells. N=5. **B.** Confocal immunofluorescence analysis of pMSK in cardiomyocytes in ventricular cardiac sections prepared from rats infused with ET-1 or Iso for 15 min. Cardiomyocyte nuclei were demarcated by pericentriolar material 1 (Pcm-1; in magenta) perinuclear staining. Nuclei are stained with DAPI (blue) and pMSK in green. Left: Quantification of nuclear pMSK in Pcm-1 positive nuclei. N=4. Right: Confocal images of heart sections from animals treated as indicated. Scale bar = 20 µm. **C.** Representative confocal images of immunostained NRVMs showing expression of FLAG-tagged WT-MSK and DN-MSK adenoviruses (AdV). Nuclei are stained with DAPI (blue, Beta-Actin in green and FLAG-tagged MSK in red. **D.** Immunoblotting for pMSK, pERK and FLAG-tagged MSK AdV in NRVMs infected with either empty vector (EV), WT-MSK1 AdV or DN-MSK1 AdV and treated +/- 15 min with ET-1, normalised to α-Act as a loading control. Left: Representative immunoblot. Right: Quantification of immunoblot, relative to EV. N=5. **E.** Immunoblotting for phosphorylated histone H3S28 in NRVMs infected with either empty vector (EV), WT-MSK1 AdV or DN-MSK1 AdV treated +/- 15 min with ET-1, normalised to total Histone 3 (T-H3) as a loading control. Left: Representative immunoblot. Right: Quantification of immunoblot data. N=6. **F.** Effect of DN-MSK expression on *c-Fos* expression in NRVM treated with ET-1 for 10 min. *c-Fos*

expression was determined by RT-qPCR. Data is presented relative to empty vector. N = 6-10. **G.** Analysis of hypertrophic responses in NRVMs infected with EV or DN-MSK1 AdV treated +/- ET-1 for 24 h. Left: RT-qPCR expression analysis of *Nppa*/*Anf* mRNA in NRVMs. Data is presented relative to EV untreated cells. N=4. Right: Cell area (μm^2) as a measure of hypertrophy in NRVMs. N=4. **H.** ChIP-qPCR analysis for pH3S28 abundance at *c-Jun* (left) and *c-Fos* gene promoter regions in NRVMs infected with EV or DN-MSK1 AdV +/- ET-1 for 10 min. Top: schematic for the site of ChIP primer amplification relative to the transcription start sites. Below: quantification of enrichment compared with EV AdV untreated NRVMs. N=4. **I**. ChIP-qPCR analysis for Brg1 enrichment at *c-Jun* (left) and *c-Fos* gene promoter regions in NRVMs infected with EV or DN-MSK1 AdV +/- ET-1 for 10 min. Quantification of Brg1 enrichment at the *c-Jun* (Left) and *c-Fos* (Right) promoters compared with EV AdV untreated NRVMs. N=4. **J.** ChIP-qPCR for Brg1 at the *c-Jun* and *c-Fos* gene promoters (left-right) in left ventricular tissue from adult male Wistar rats that were administered ET-1 or Iso through jugular vein administration and sacrificed 15 min later. N=3.

Figure S3: IEG activation is a conserved feature of hypertrophy in adult cardiomyocytes

A. Confocal images of immunostained ARVMs infected with adenovirus expressing FLAG-tagged DN-Msk (kinase dead). ARVMs are stained for FLAG (green), pH3S28 (red) and β-Act (purple). FLAG-tagged DN-Msk is enriched in the nuclei in ARVMs. **B.** RT-qPCR analysis of *c-Fos* (Top) and *Nppa*/Anf (Bottom) mRNA in ARVMs infected with EV or DN-MSK1 +/- ET-1 treatment for 15 min. N=4. Scale bar = 25 µm. **C.** Analysis of siRNA-mediated knockdown of *Msk1* in NRVMs. RT-qPCR analysis of *Msk1* mRNA expression in NRVMs transfected with scr or siMsk siRNA is shown. **D.**

RT-qPCR analysis of *c-Fos* mRNA in NRVMs transfected with scr or siMsk siRNA +/- ET-1 for 15 min. N=4. **E.** RT-qPCR analysis of *Nppa/Anf* mRNA expression in NRVMs transfected with scr or siMsk siRNA +/- ET-1 for 15 min. N=4. **F.** Analysis of *Smarca4* knockdown in NRVMs. *Smarca4/Brg1* mRNA abundance was measured by RT-qPCR in NRVMs transfected with siRNA targeting Smarca3 (siBrg1) and compared with NRVMs transfected with scrambled control (scr) siRNA. N=3. **G.** RT-qPCR analysis of *Myh6/Myh7* (Left) and *c-Fos* (Right) mRNA expression in NRVMs transfected with scr or siBrg1 siRNA +/- ET-1 for 15 min. N=5. **I.** ChIP-qPCR for pH3S28 at the *c-Fos* promoter region in NRVMs transfected with scr or siMsk siRNA +/- ET-1 for 15 min. N=5.

Figure 4: Genetic MSK inhibition attenuates IEG activation and cardiomyocyte hypertrophy in vivo

A. RT-qPCR analysis of *Msk1* (Left) and *Msk2* (Right) mRNA expression in left ventricle from *Msk1/2* KO mice and wild type littermates +/- Iso infusion for 1 week. N=5, WT Iso, N=4, KO ctrl, N=5, KO Iso, N=5. **B.** RT-qPCR analysis of expression of IEGs *c-Jun* (Left) and *c-Fos* (Right) in left ventricle from *Msk1/2* KO mice and wild type littermates +/- Iso infusion for 1 week. WT ctrl, N=5, WT Iso, N=4, KO ctrl, N=5, KO Iso, N=5. **C.** RT-qPCR analysis of *Smarca4/Brg1* mRNA expression in left ventricle from *Msk1/2* KO mice and wild type littermates +/- Iso infusion for 1 week. N=5, WT Iso, N=4, KO ctrl, N=5, KO Iso, N=5. **D.** Immunostaining for pMSK in cardiomyocyte nuclei in left ventricular cardiac sections in *Msk1/2* KO mice and wild type littermates +/- Iso infusion for 1 week. Cardiomyocyte nuclei are demarcated with Nesprin. Left: Quantification of pMSK in Nesprin+ve nuclei. Right: Representative immunostaining images for pMSK (green), Nesprin (red) and nuclei are stained with DAPI (blue). N=4.

Scale bar = 50 µm. **E.** Immunostaining for pH3S28 in cardiomyocyte nuclei in left ventricular cardiac sections in *Msk1/2* KO mice and wild type littermates +/- Iso infusion for 1 week. Cardiomyocyte nuclei are demarcated with Pcm-1. Left: Quantification of pH3S28 in Pcm-1+ve nuclei. Right: Representative immunostaining images for pH3S28 (red), Pcm-1 (green) and nuclei are stained with DAPI (blue). N=4. Scale bar = 50 µm. **F.** Fractional shortening in *Msk1/2* KO mice and wild type littermates at baseline (Iso=0) and +/- Iso infusion for 1 week (Iso=1), derived from 2D echocardiography data. WT ctrl, N=6, WT Iso, N=4, KO ctrl, N=5, KO Iso, N=6. **G.** Posterior wall dimension in diastole in *Msk1/2* KO mice and wild type littermates at Iso=0 and +/- Iso=1, derived from 2D echocardiography data. WT ctrl, N=6, WT Iso, N=4, KO ctrl, N=5, KO Iso, N=6. **H.** RT-qPCR analysis of the markers of pathological hypertrophy *Nppa*/Anf, *Nppb*/Bnp and *Myh*7 mRNA expression in left ventricle from *Msk1/2* KO mice and wild type littermates +/- Iso infusion for 1 week. N=5, WT Iso, N=4, KO ctrl, N=5, KO Iso, N=5. **I.** Quantification of left ventricular interstitial fibrosis, measured as percentage (%) area of extracellular matrix from Picro Sirius Red staining in left ventricular tissue from *Msk1/2* KO mice and wild type littermates +/- Iso infusion for 1 week. N=5, WT Iso, N=4, KO ctrl, N=5, KO Iso, N=5. **J.** RT-qPCR analysis of *Col1a1* mRNA expression in left ventricular tissue from *Msk1/2* KO mice and wild type littermates +/- Iso infusion for 1 week. WT ctrl, N=5, WT Iso, N=4, KO ctrl, N=5, KO Iso, N=5.

Figure S4: Genetic MSK inhibition attenuates IEG activation and cardiomyocyte hypertrophy in vivo

A. Heat map showing expression of immediate early gene (*c-Jun, c-Fos, FosL1, FosB, JunD*), *Smarca4/Brg1, Erk1/2* and *Msk1/2* in left ventricular Pcm-1+ve cardiomyocyte

RNA-seq data in models of pathological (Ascending aortic banding, AB) or physiological (treadmill training, run) in male Sprague Dawley rats. Data extracted from (Thienpont et al., 2017). **B.** RT-qPCR analysis of *Msk1* and *Msk2* mRNA expression in NRVMs treated with ET-1 for 15 min. N=5. **C.** Representative M-mode echocardiogram from WT/*Msk* KO mice +/- Iso for 1 week. Echocardiographic measurements indicated. IVSd=Interventricular septal dimension end systole, IVSd=Interventricular septal dimension end diastole, LVDs=Left ventricle diameter end systole, LVDd=Left ventricular diameter end diastole, PWd=posterior wall dimension end diastole, PWs=posterior wall dimension end systole. **D.** Representative left ventricular tissue sections from WT/*Msk* KO mice +/- Iso for 1 week showing Picro sirius red staining for collagen. The scale bar indicates 50 µm. **E.** Terminal deoxynucleotidyl transferase dUTP nick end labelling (TUNEL) staining of left ventricular cardiac sections in *Msk1/2* KO mice and wild type littermates +/- Iso infusion for 1 week. TUNEL assay measures fragmented DNA as a mark of apoptosis. Left: Quantification of TUNEL in cardiac nuclei. Right: Representative immunostaining images for TUNEL (green) and nuclei are stained with DAPI (blue). N=3. The scale bar indicates 20 µm. **F.** RT-qPCR analysis of pro-apoptotic marker genes caspase 3 (Casp3), caspase 9 (Casp9) mRNA expression in left ventricle from *Msk1/2* KO mice and wild type littermates +/- Iso infusion for 1 week. WT ctrl, N=5, WT Iso, N=4, KO ctrl, N=5, KO Iso, N=5. **G.** RT-qPCR analysis of the expression of the anti-apoptotic marker gene *Bcl2* mRNA expression in left ventricle from *Msk1/2* KO mice and wild type littermates +/- Iso infusion for 1 week. WT ctrl, N=5, WT Iso, N=4, KO ctrl, N=5, KO Iso, N=5.

Figure 5: The MAPK-MSK-pH3S28 axis is conserved in the hypertrophic response in humans.

A. Confocal immunofluorescence analysis of pH3S28 in isolated human donor cardiomyocytes treated for 15 min with ET-1 or Iso +/- PD. Left: Quantification of immunostaining of nuclear pH3S28. Right: Representative images of isolated cardiomyocytes stained for pH3S28 (red), α-Act (cyan), nuclei stained with DAPI (blue). N=4. Scale bar = 20 µm. **B.** Confocal immunofluorescence analysis of pMSK in isolated Immunostaining in isolated human donor cardiomyocytes treated for 15 min with ET-1 or Iso +/- PD. Left: Quantification of immunostaining of nuclear pMSK. Right: Representative images of isolated cardiomyocytes stained for pMSK (green), α-Act (purple), nuclei stained with DAPI (blue). N=4. Scale bar = 20 µm. **C-E.** RT-qPCR analysis of mRNA expression of indicated genes in human hypertrophic left ventricular tissue (H) compared with non-failing (C). C, N=5, H, N=4. **C.** RT-qPCR analysis of *MSK1* and *MSK2* mRNA expression. **D.** RT-qPCR analysis of expression of immediate early gene components of the AP-1 transcription factor. **E.** RT-qPCR analysis of *SMARCA4* (*BRG-1)*. **F.** ChIP-qPCR analysis for pH3S28 enrichment at the *c-JUN* and *c-FOS* promoters in Pcm-1 +ve cardiomcyocyte nuclei from human hypertrophic left ventricular tissue (H) compared with non-failing (C). N=3. **G.** ChIP-qPCR for pH3S28 enrichment at the *SMARCA4/BRG-1* promoter in Pcm-1 +ve cardiomcyocyte nuclei from human hypertrophic left ventricular tissue (H) compared with non-failing (C). N=3.

Figure 6: Summary cartoon of main findings of this study indicating pathway by which MSK couples GPCR activation with IEG induction during the cardiac hypertrophic response

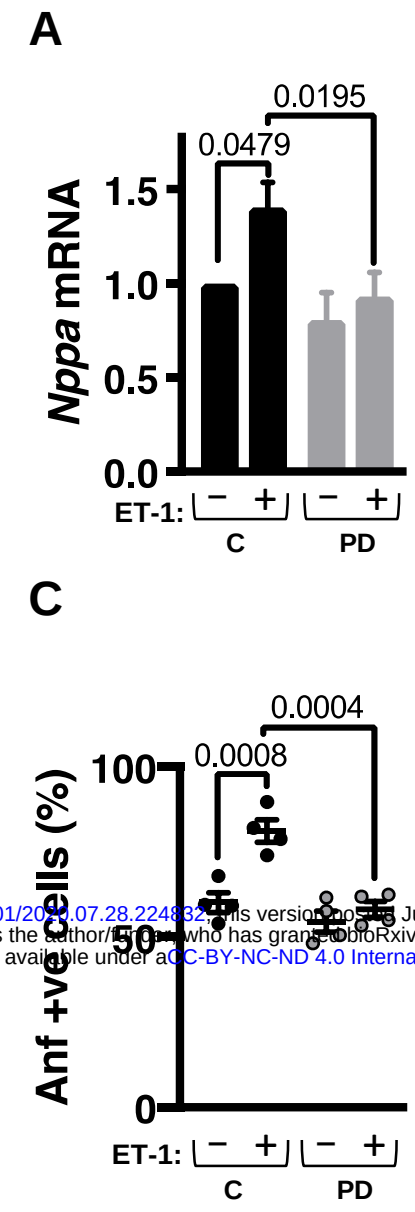

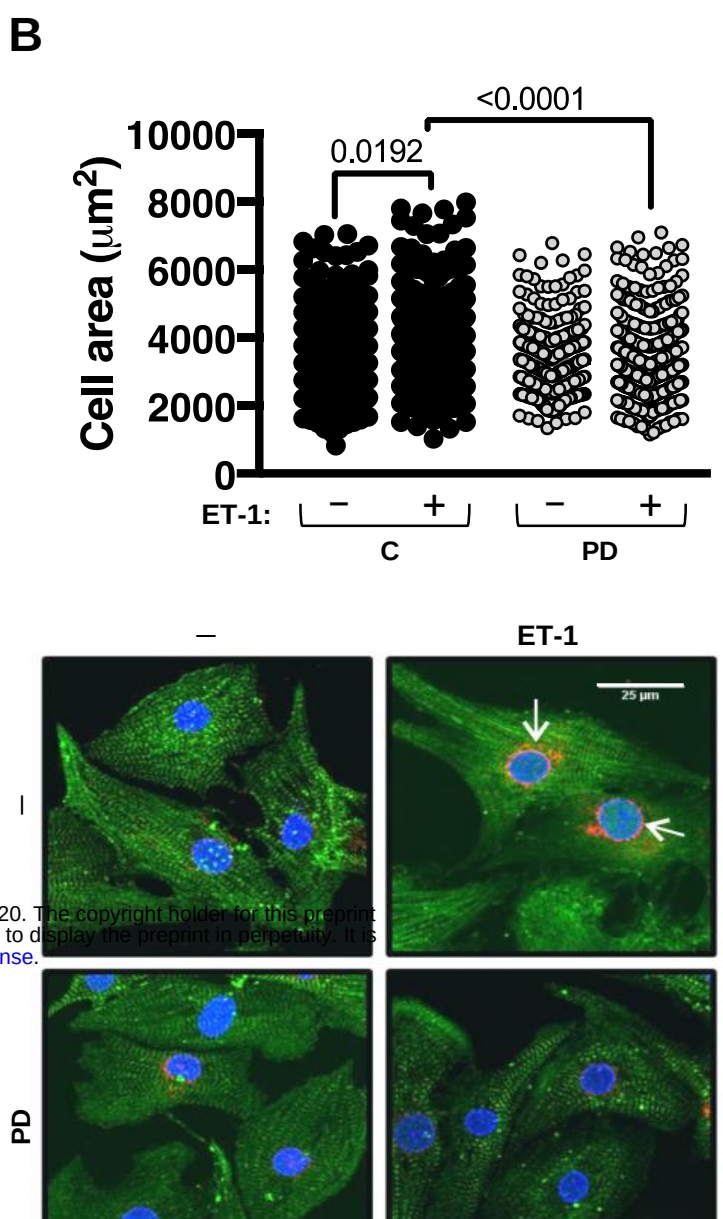

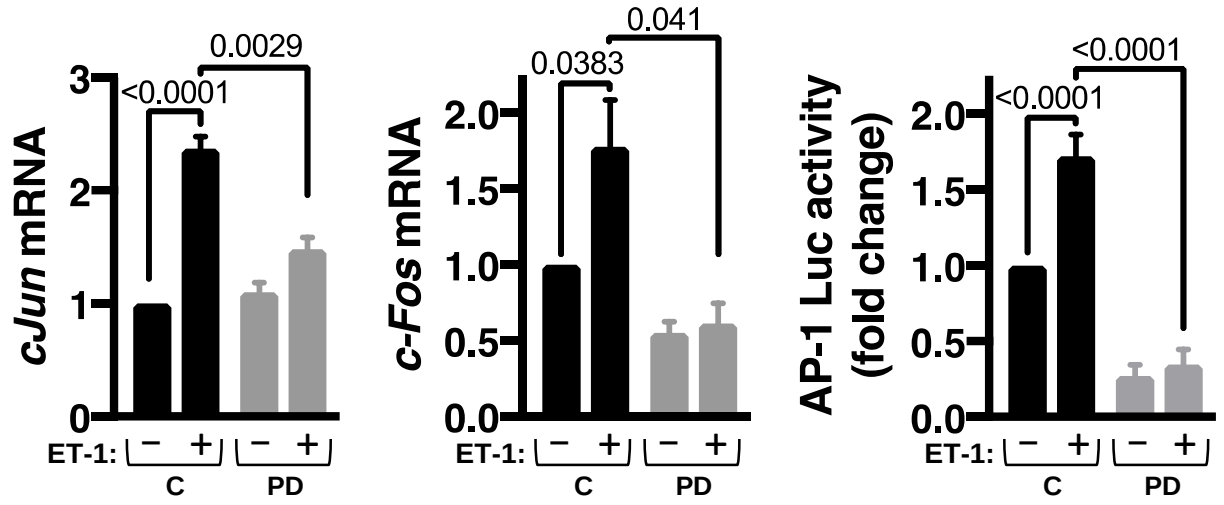

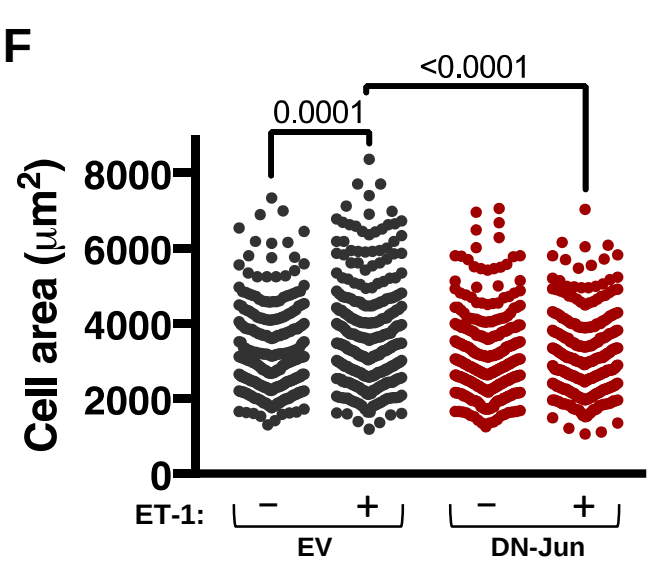

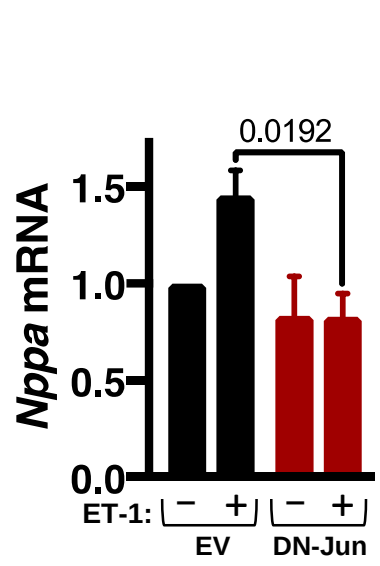

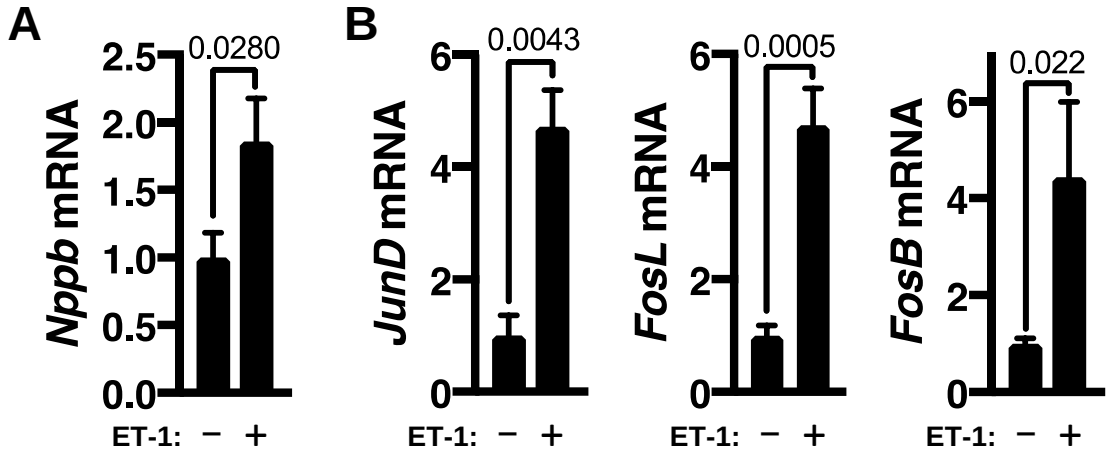

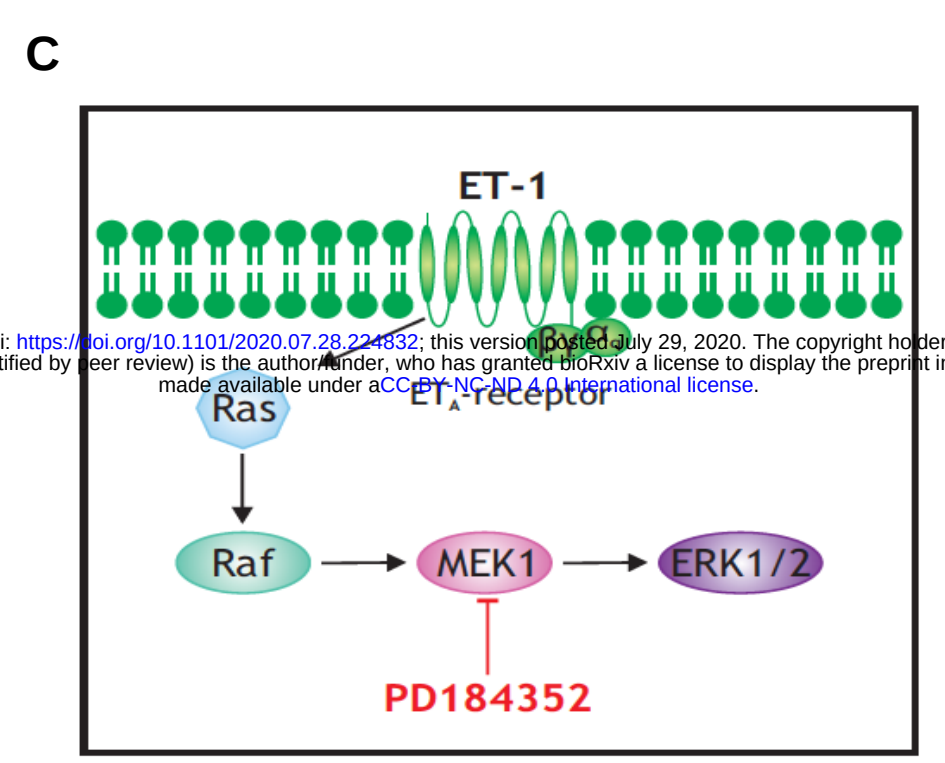

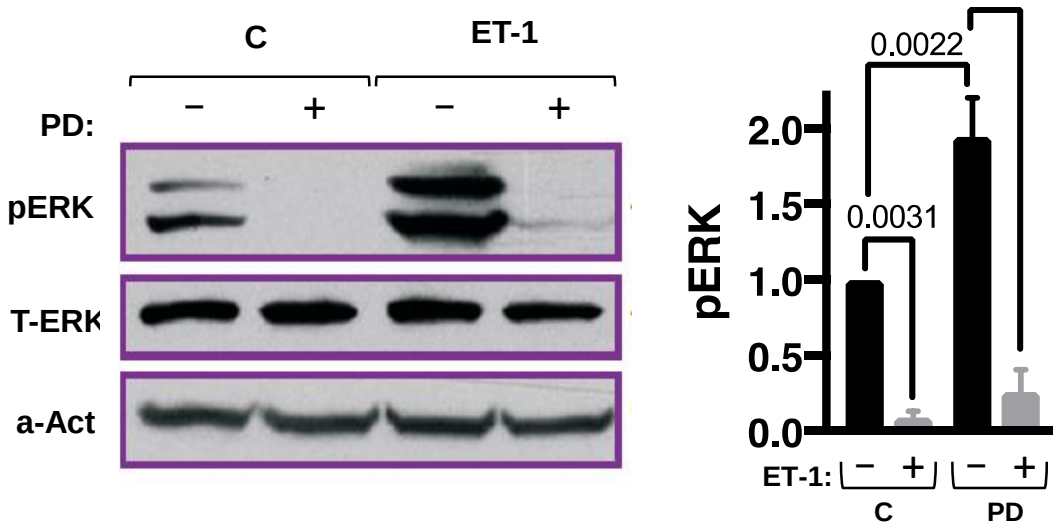

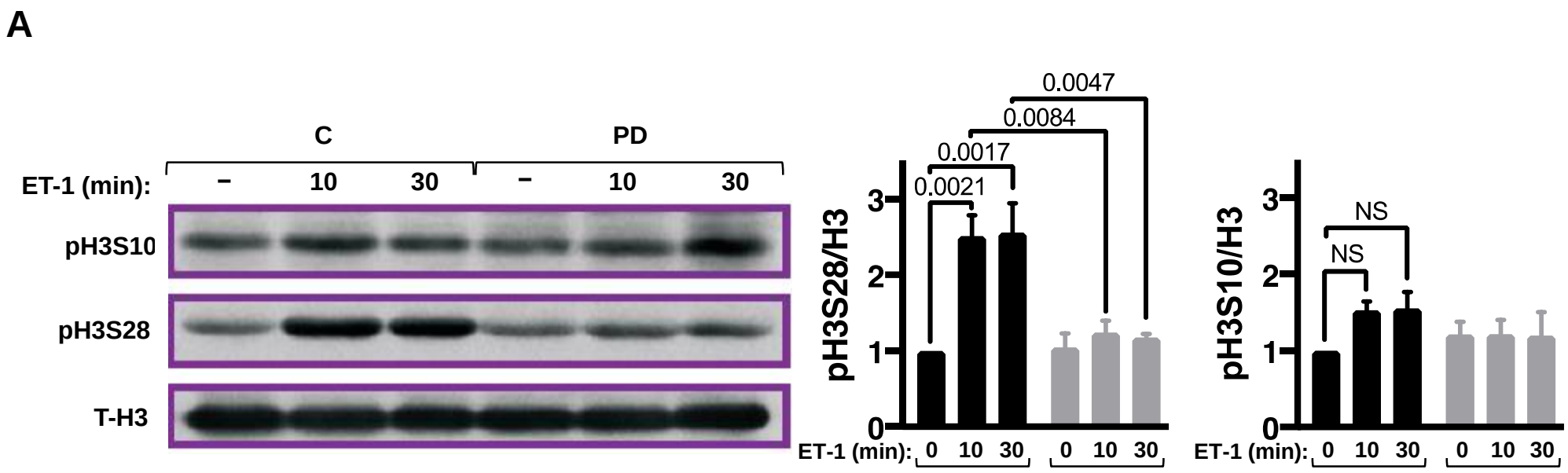

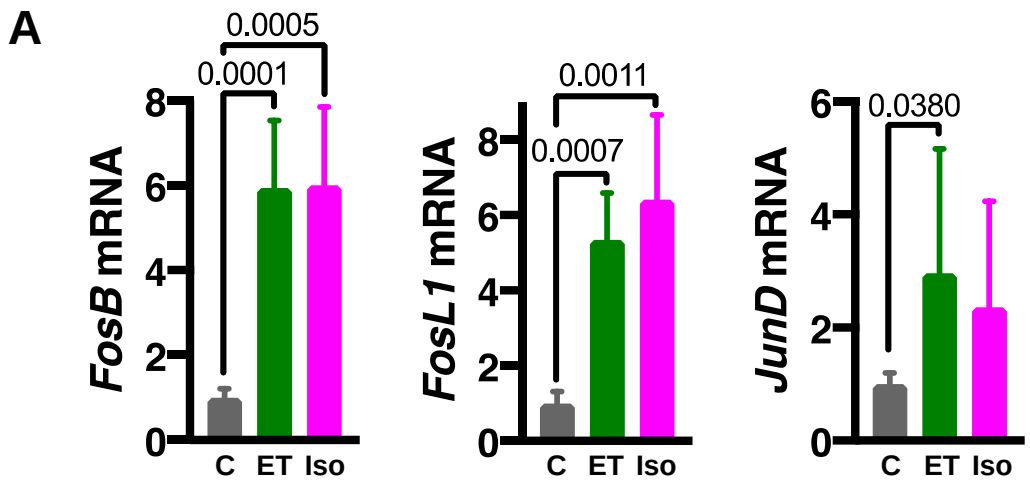

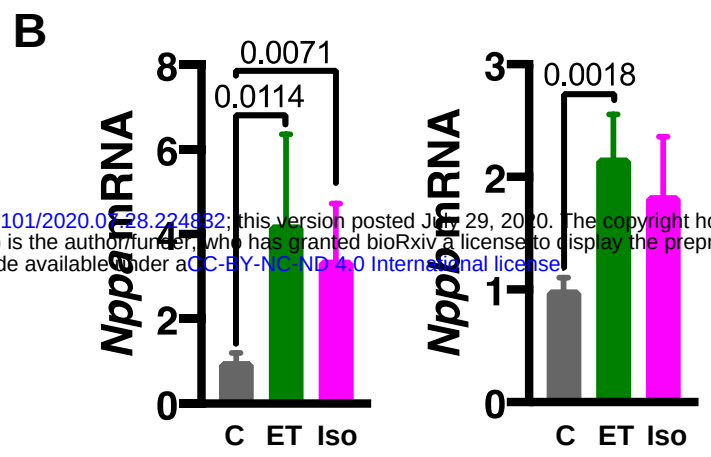

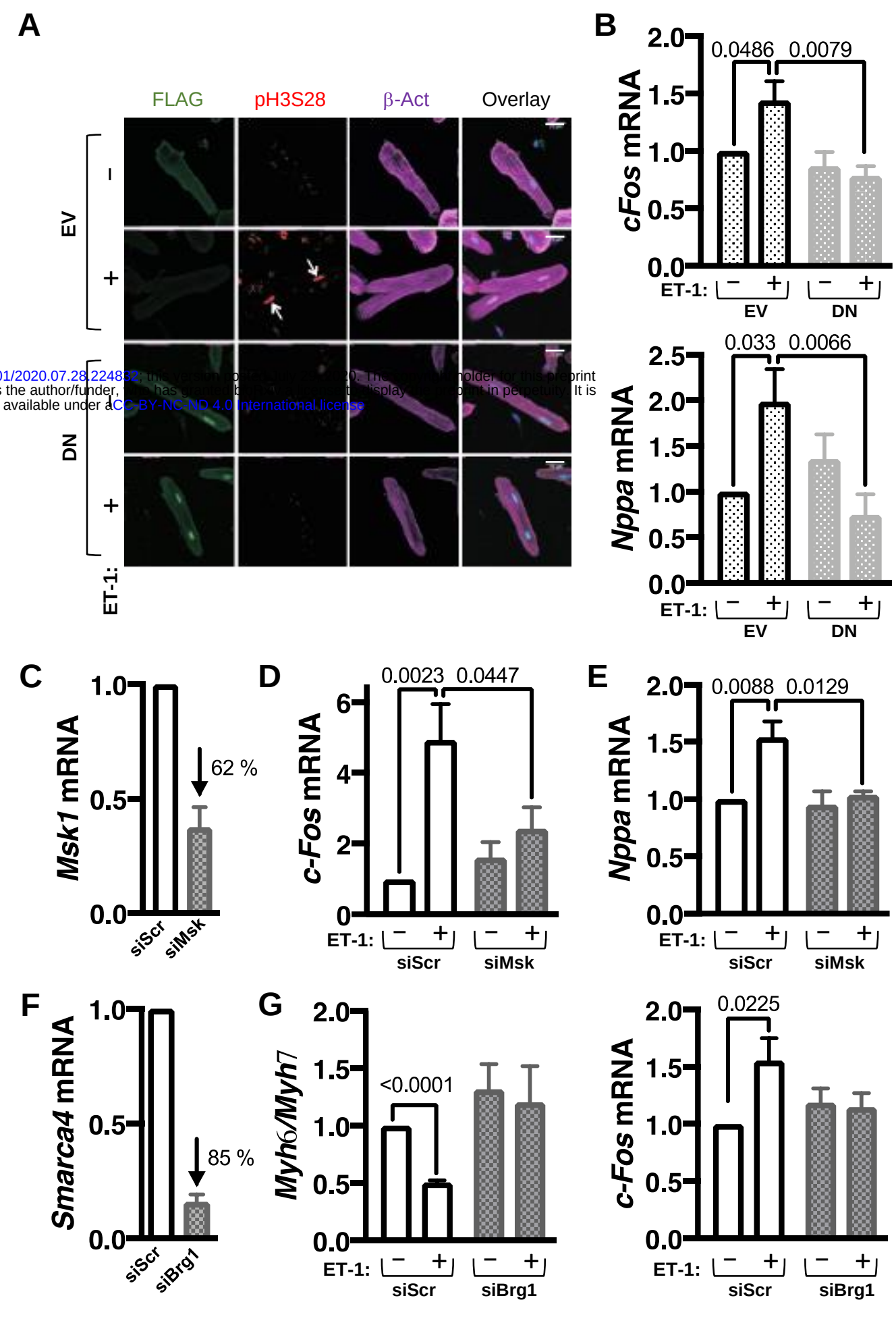

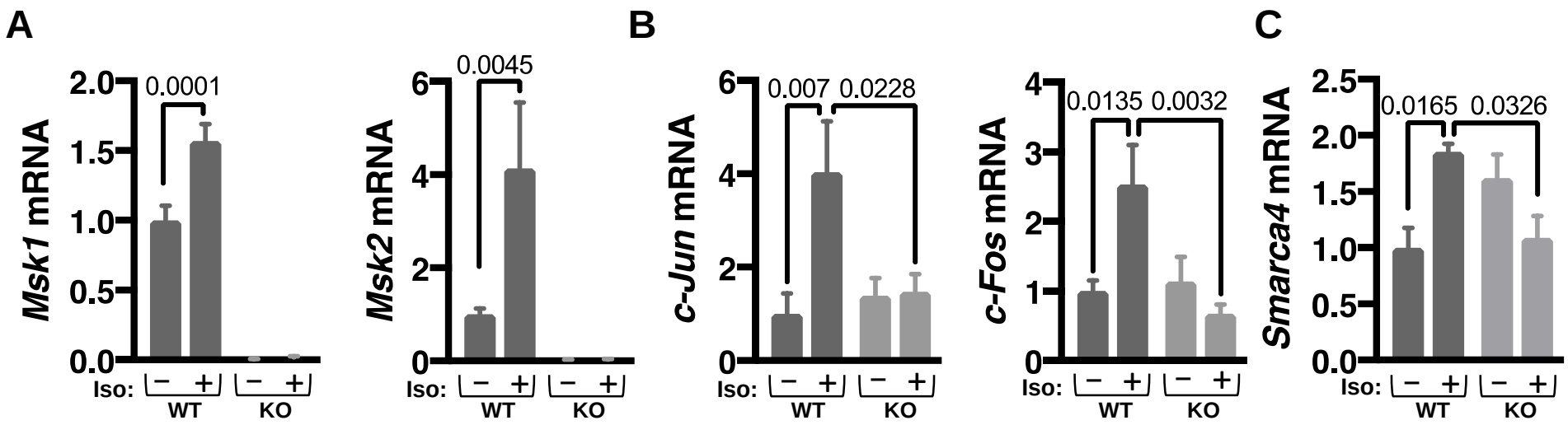

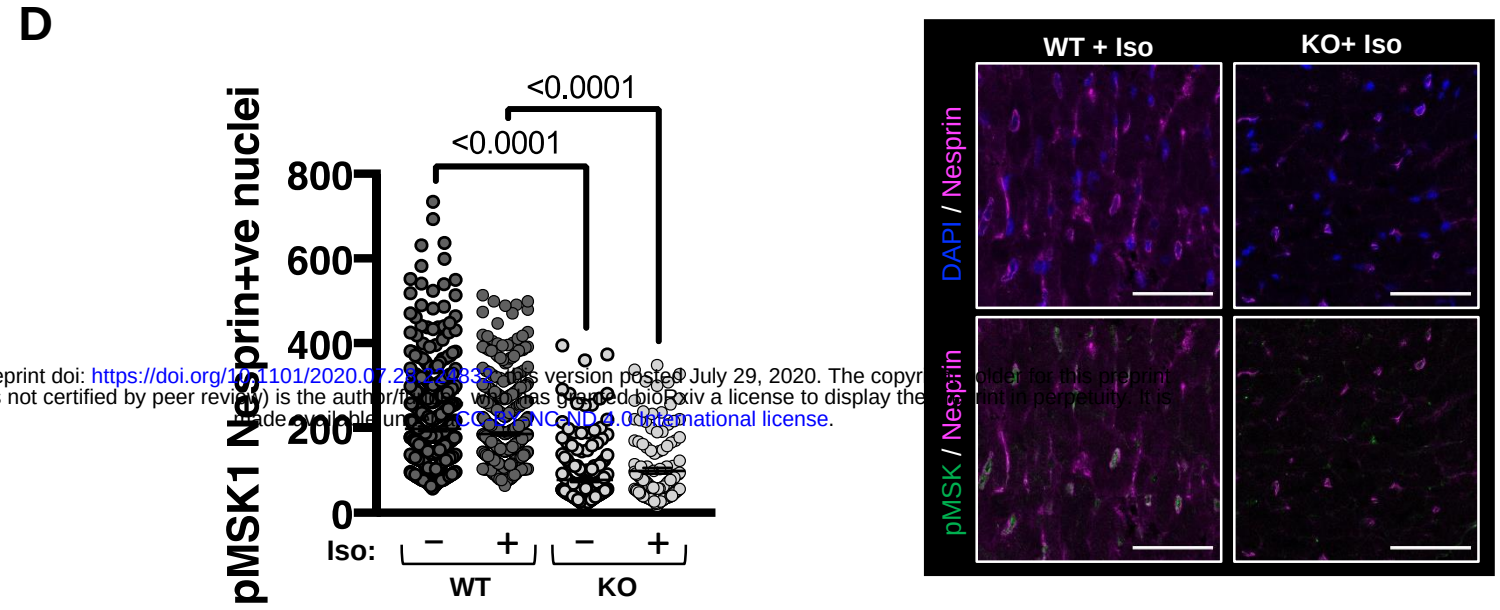

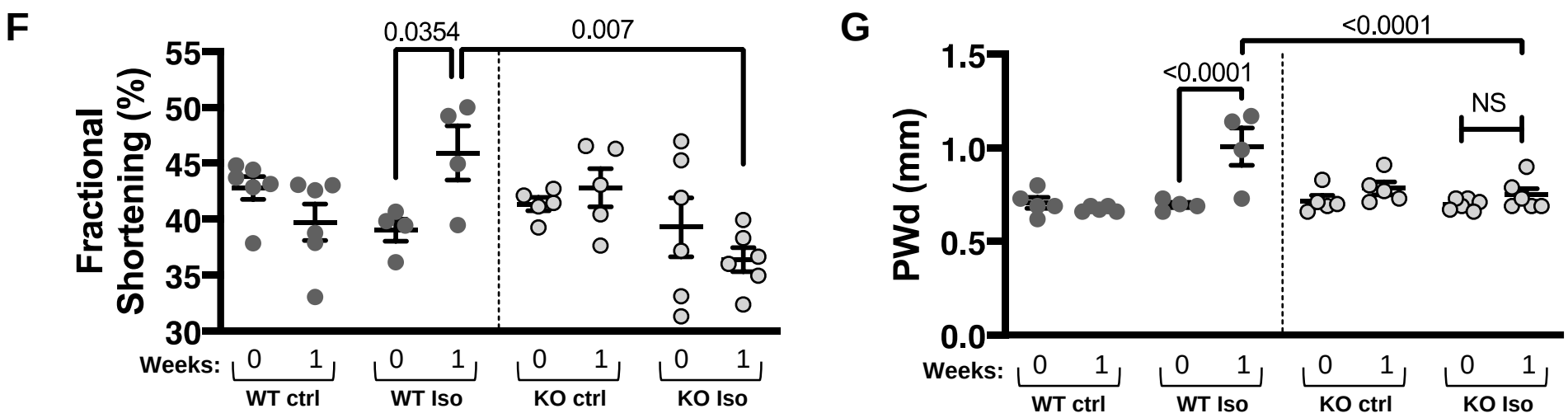

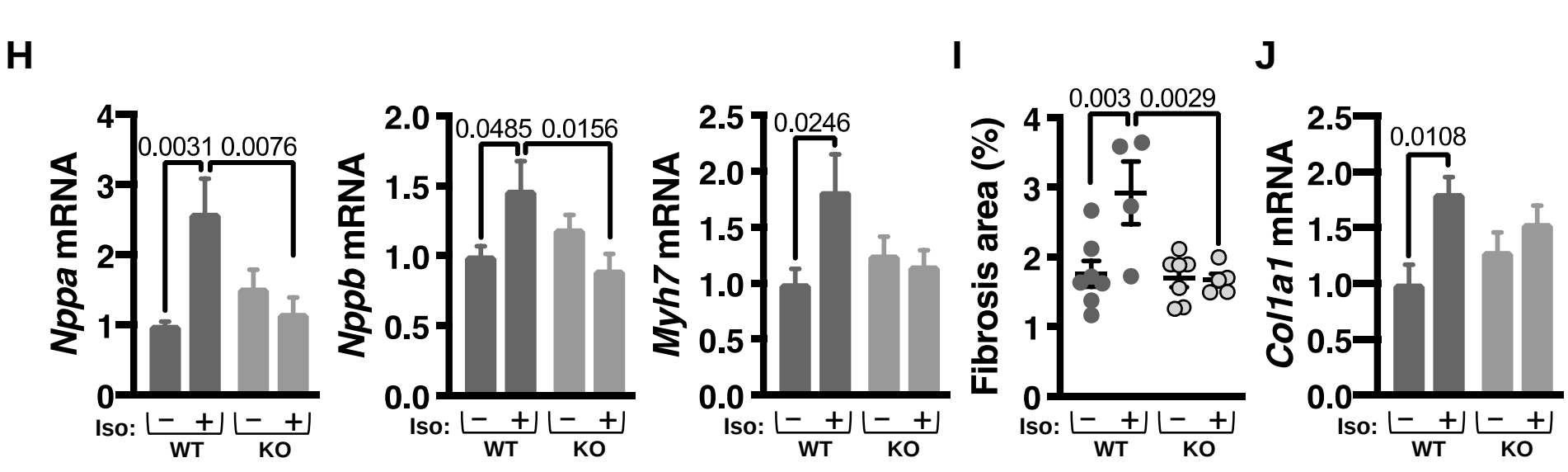

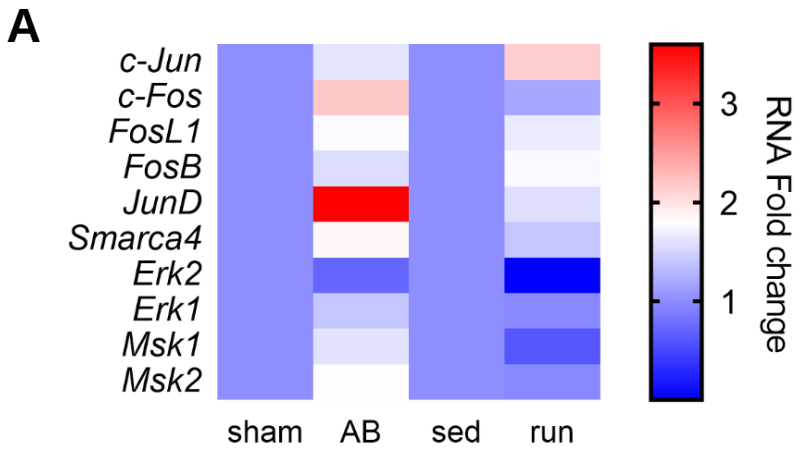

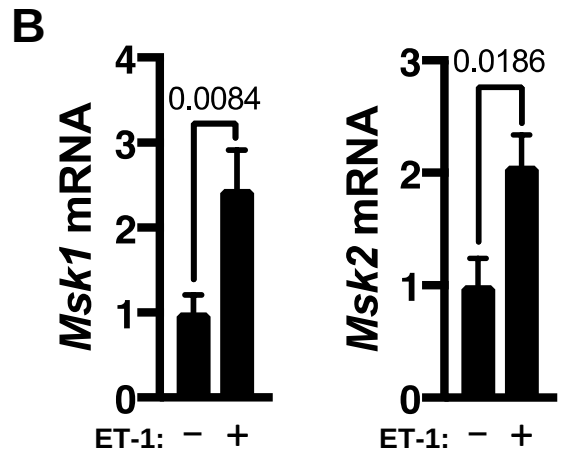

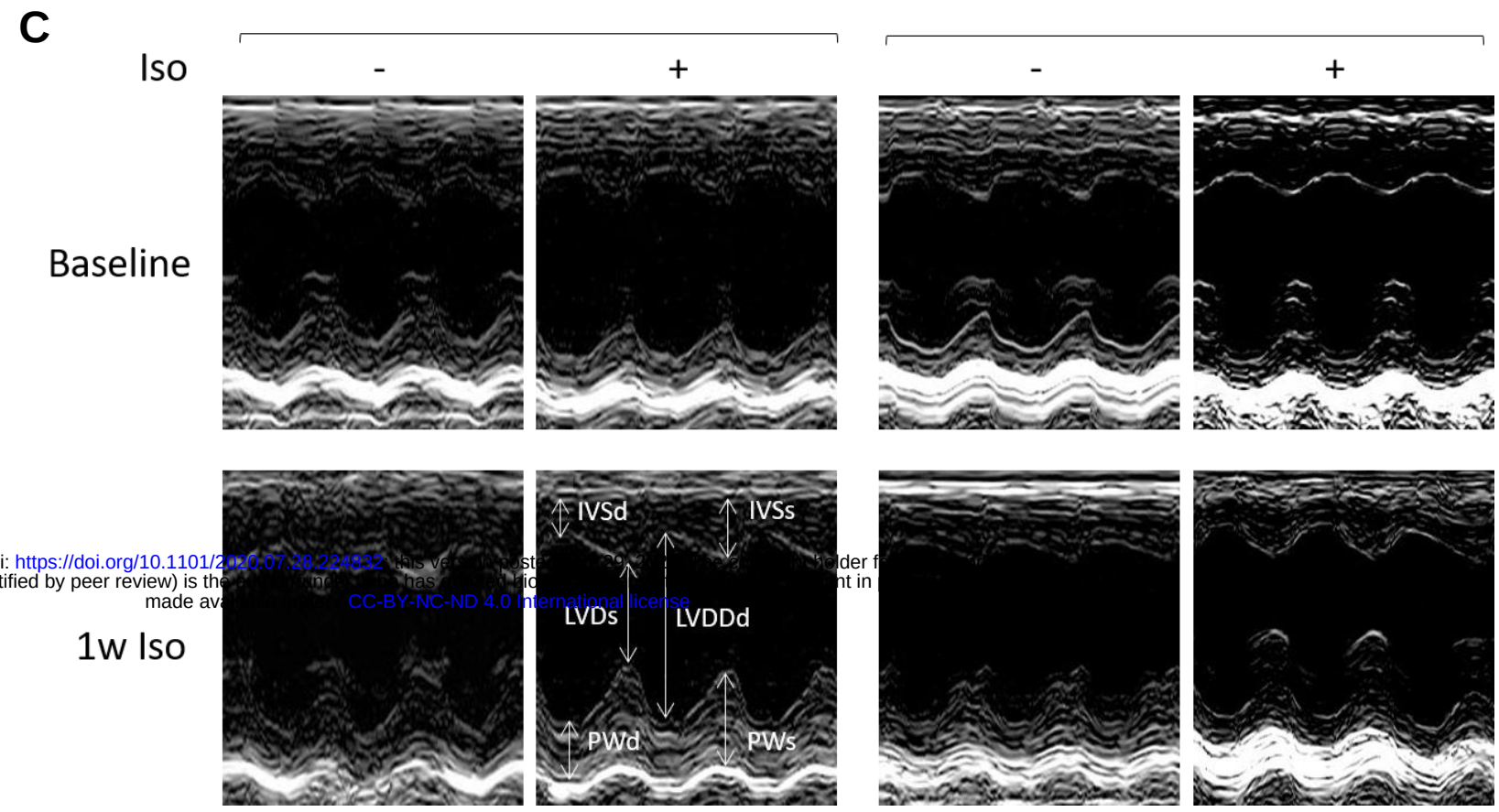

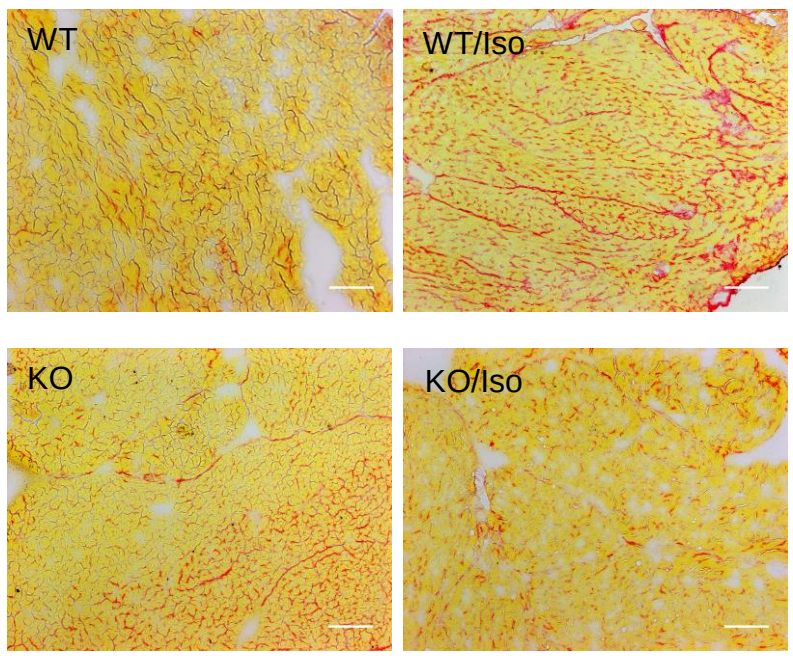

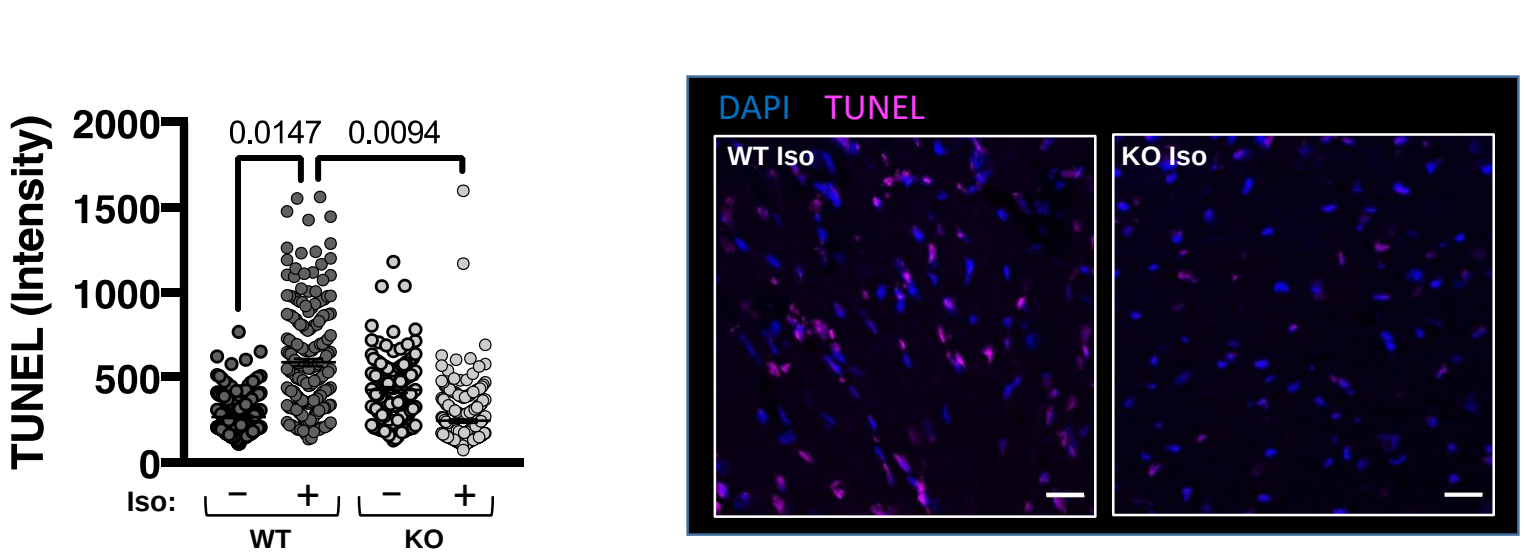

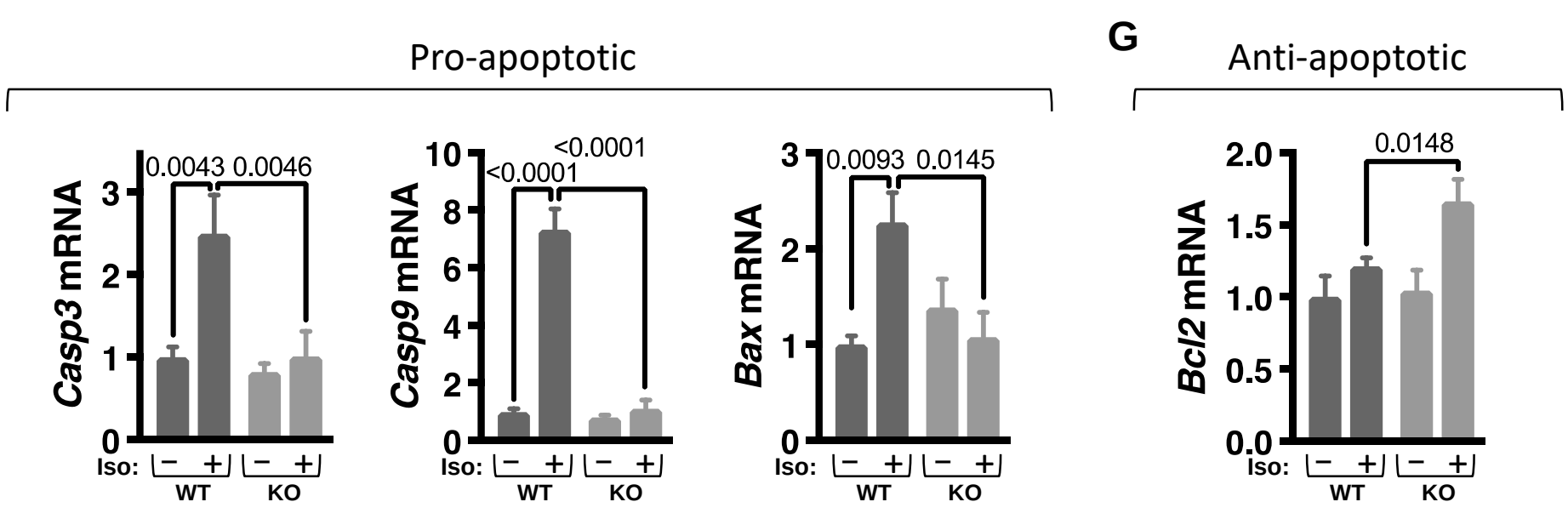

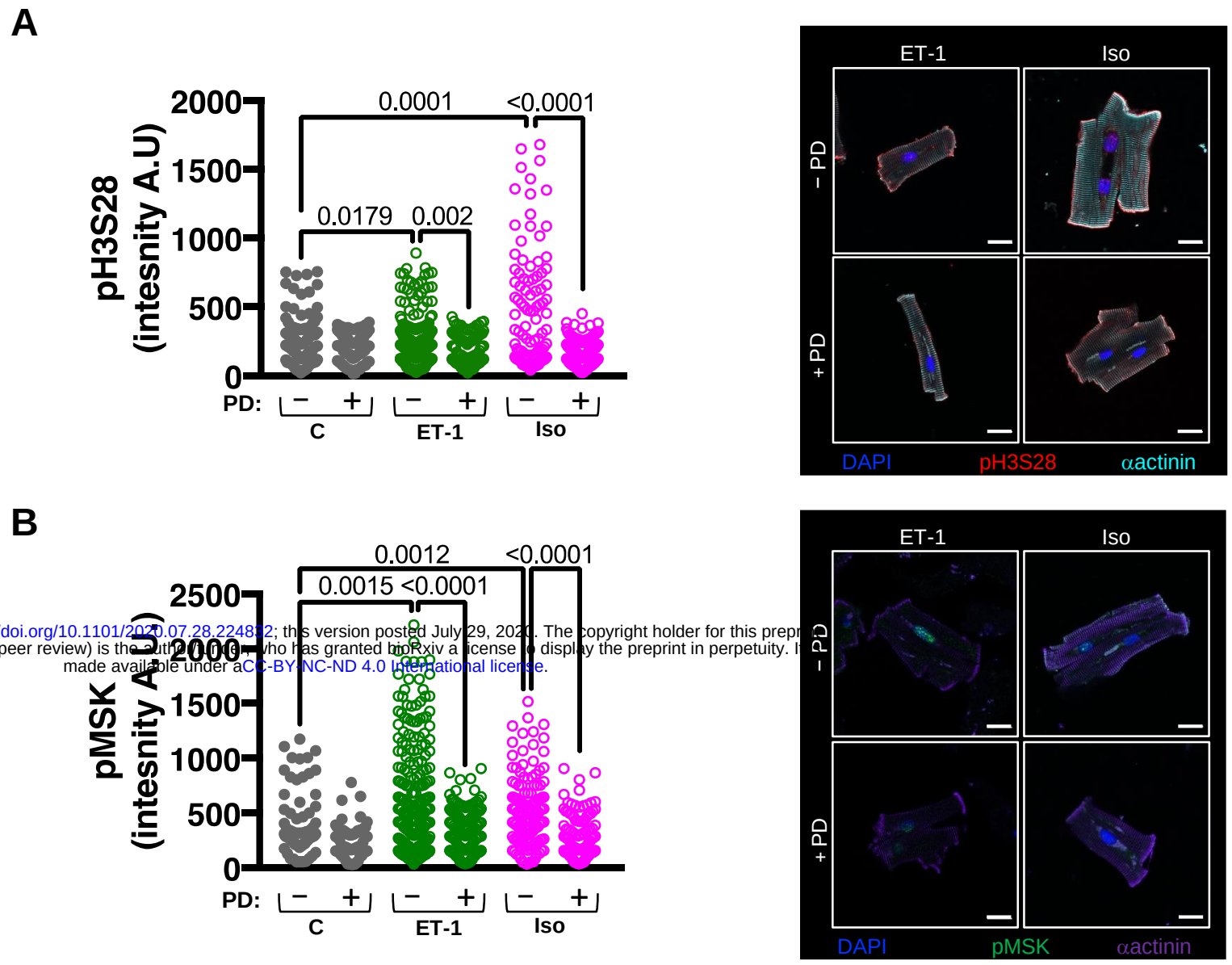

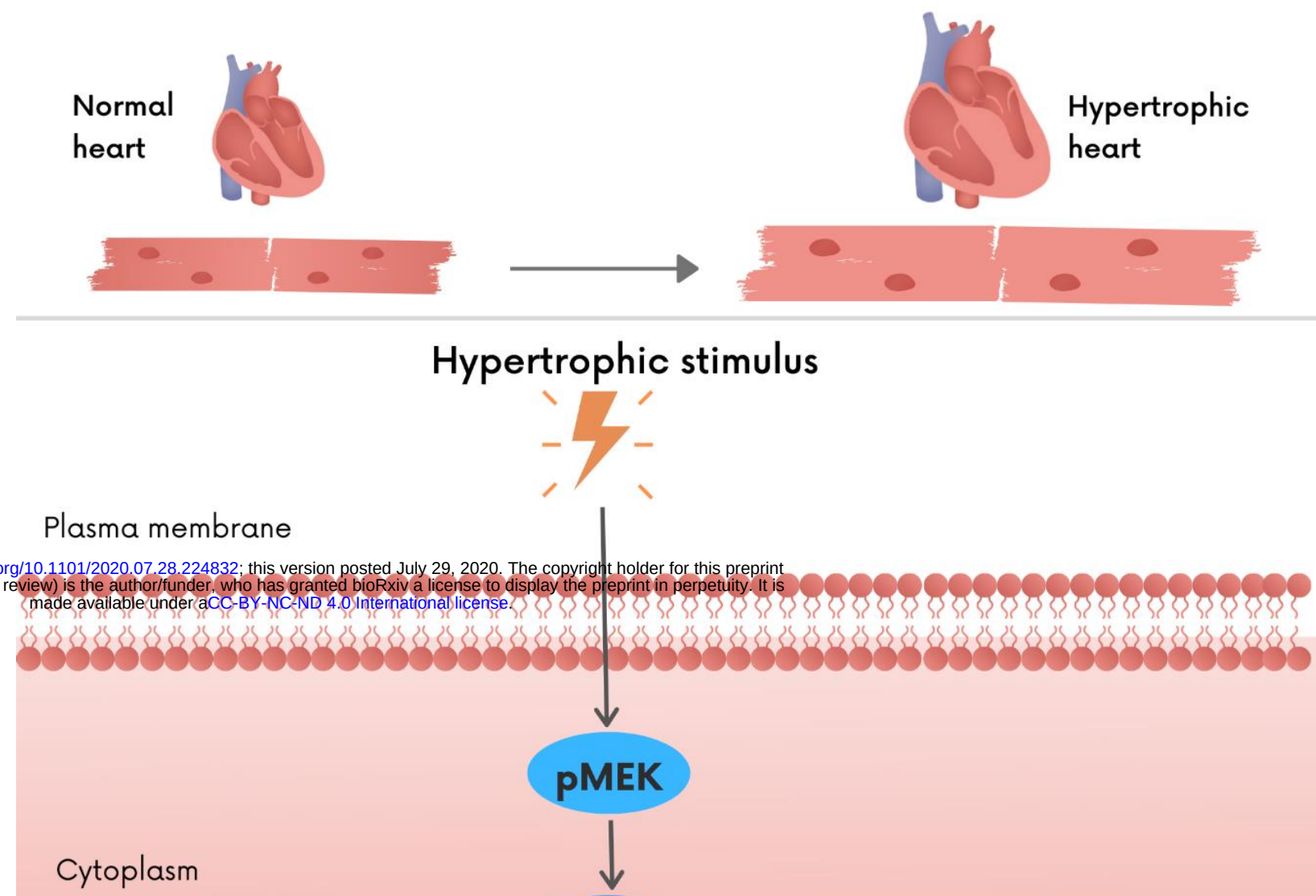

Supplementary Data

Table S1: Human healthy donor samples for cardiomyocyte isolation

Patient	Age	Sex	BMI	Medications
HD-13	78	F	23	Antidiuretics, Insulin, corticosteroids
HD-19	57	F	23	Noradrenalin, Insulin, corticosteroids, T3
HD-20	74	F	31	Antibiotics, corticosteroids
HD-30	73	F	23	Noradrenalin, Dopamine, Insulin, corticosteroids

Samples used in Table S1 were used to generate data in Figures 5A-B.

Table S2: Human control and hypertrophic left ventricular cardiomyocyte nuclei

Sample I.D.	Age (yrs)	B.M.I.	Heart Mass (g)	Pathology/Cause of Death
ND231	57	21.9	320	Control/multiple injuries, fall down from 4th floor.
ND241	43	32.2	590	left ventricular hypertrophy/natural
ND248	57	21.7	460	Control/suicide
ND249	31	22	343	Control/suicide
ND251	39	33.7	582	Control/Intoxication
ND252	37	20	496	left ventricular hypertrophy/natural
ND259	60	23.7	400	Control/intoxication
ND279	61	29	710	left ventricular hypertrophy/natural
ND288	63	30	563	left ventricular hypertrophy/intoxication

Samples in Table S2 were used to generate data in Figure 5C-F.

Table S3: Antibody order information and concentrations

IF = immunofluorescence, IB = immunoblotting

Antibody	Order Information	Technique	Dilution Used
ANF	Bachem T-4014	IF	1:500
pERK	Cell signalling technology (CST), 9106S	IB	1:1000
T-ERK	BD Biosciences, 610031	IB	1:5000
α-Actinin	Sigma Adrich, A7811	IB	1:2000
		IF	1:100

B-Actin	Abcam, 52219	IF	1:1000
Histone3	Sigma Aldrich, H0164	IB	1:10 000
Phos H3S10	CST, 9701S	IB	1:1000
Phos H3S28	Sigma Aldrich, H9908	IB	1:2000
		IF	1:1000
Phos H3S28	Millipore, 07-145	ChIP	1:100
PCM1	Sigma Aldrich Prestige, HPA023370	IF	1:500
Nesprin1	MANNES1A (7A12) kindly donated to use by Glenn Morris) (1)	IF	1:100
pMSK	CST, 9591S	IB	1:1000
cFos	Abcam, ab190289	IF	1:250
FLAG	Sigma Aldrich, FF3165	IB	1:2000
		IF	1:100
Secondary Antibodies			
HRP-conjugated antibodies	Jackson Laboratories	IB	1:10 000
Alexa 488	Life Technologies, R37116, A-11029	IF	1:500
Alexa 568	Life Technologies, A-11036	IF	1:500
Alexa 647	Life Technologies, A-21244	IF	1:500

Table S4: Primer sequence information

Primers were ordered from Sigma Aldrich or Integrated DNA Techologies as lyophilized custom oligos, purified by desalting.

Gene target	Species	Sequence
RTqPCR		
GAPDH	Rat	F-CAAGATGGTGAAGGTCGGTGT R-GGTCGTTGATGGCAACAATG
	Mouse	F-AATGGTGAAGGTCGGTGTGAAC R-TCGTTGATGGCAACAATCTCC
	Human	F-GAGTCAACGGATTTGGTCGT R-GACAAGCTTCCCGTTCTCAG
TBP	Rat	F-TGACTCCTGGAATTCCCATC R-TGTGTGGGTTGCTGAGATGT
	Mouse	F-GGGGAGCTGTGATGTGAAGT R-CAGGAGAACATGGCAGACAA
	Human	F-TATAATCCCAAGCGGTTTGC R-GCTGGAAAACCCAACTTCTG
YWHAZ	Rat	F-ACCCACTCCGGACACAGAAT

		R- AGGCTGCCATGTCATCGTA
	Mouse	F-CAGAAGACGGAAGGTGCTGAGA R-CTTTCTGGTTGCGAAGCATTGGG
	Human	F-CGAGATCCAGGGACAGAGTC R-GGATGTTCTGTGTCCGGAGT
18S	Rat/Mouse	F-ATCCATTGGAGGGCAAGTC R-CGCTCCCAAGATCCAACTAC
	Human	F-AAACCACAGGCAAACACCTC R-GCACTTTGGGTGGTCAAGTT
RPL32	Rat/Mouse	F-GGCCAGATCCTGATGCCCAAC R-CAGCTGTGCTGCTCTTTCTAC
	Human	F-AGGCATTGACAACAGGGTTC R-GACGTTGTGGACCAGGAACT
SDHA	Rat	F-TCGCACTGTGCATAGAGGAC R-ATGCCTGTAGGGTGGAACTG
	Mouse	F-AAGGCAAATGCTGGAGAAGA R-TGGTTCTGCATCGACTTCTG
	Human	F-TCGCACTGTGCATAGAGGAC R-GCCTGTAGGGTGGAACTGAA
LMNA	Rat	F-TGAGTACAACCTGCGCTCAC R-TGTGACACTGGAGGCAGAAG
	Mouse	F-GCACCGCTCTCATCAACTCC R-TCTTCTCCATCCTCGTCGTCA
	Human	F-CTACACCAGCCAACCCAGAT R-GGTCGAAGGACAGAGACTGC
Tuba 6	Mouse	F-GGCAGTGTTCGTAGACCTGGA R-TTATTGGCAGCATCCTCCTTG
cFOS	Rat	F-CCGACTCCTTCTCCAGCATG R-GTGGAGATGGCTGTCACCGT
	Mouse	F-GGGAATGGTGAAGACCGTGTCA R-GCAGCCATCTTATTCCGTTCCC
	Human	F-GCCTCTCTTACTACCACTCACC R-AGATGGCAGTGACCGTGGGAAT
cJUN	Rat	F-TTGAAAGCGCAAAACTCCGA R-GTTAGCATGAGTTGGCACCC
	Mouse	F-CAGTCCAGCAATGGGCACATCA R-GGAAGCGTGTTCTGGCTATGCA
	Human	F-CCTTGAAAGCTCAGAACTCGGAG R-TGCTGCGTTAGCATGAGTTGGC
JUND	Rat	F-g a c a t g g a c a c g c a g g a a c R-t c t g g c t t t t g a g g g t c t t g
	Human	F-ATCGACATGGACACGCAGGAGC R-CTCCGTGTTCTGACTCTTGAGG
FOSB	Rat	F-a a a c a a a c a a a a c c g c a a g g R-g g c g g t c a g a c a g a a g a g t c
	Human	F-TCTGTCTTCGGTGGACTCCTTC R-GTTGCACAAGCCACTGGAGGTC
FOSL	Rat	F-a g a g c t g c a g a a g c a g a a g g R-g c t g g t a c c a c c t g t g t c c t

	Human	F-GGAGGAAGGAACTGACCGACTT R-CTCTAGGCGCTCCTTCTGCTTC
SMARCA4/BRG1	Rat	F-CTACAGGAGCGGGAGTACAG R-TGGTTGCTTTGGTTCGAAGG
	Mouse	F-GAAAGTGGCTCTGAAGAGGAGG R-TCCACCTCAGAGACATCATCGC
	Human	F-CAAAGACAAGCACATCCTCGCC R-GCCACATAGTGCGTGTTGAGCA
MSK1	Rat	F-TCTATGTTGGAGAGATCGTGCTTG R-AATCTGTCAGCACCACATGGC
	Mouse	F-TGGTCCATAGCACCTCTCAGCT R-CTCTCCGCCATTCAGAAGTTCC
	Human	F-CCTGGAACACATTAGGCAGTCG R-CACCTCATGCTCTGTGAAACGC
MSK2	Rat	F-ATCCTGGACTATGTGAGCGG R-CTAGGGCCAGCACAATCTCT
	Mouse	F-CAACGTGGTGAATCTGCATGAGG R-AGCCGCTTCTTGCGGATGTGTT
	Human	F-TGTGGGCAACTTTGCGGAGGAA R-GAGAATGGAGGGTGCCACAAAG
MYH6	Rat	F-ACAGAGTGCTTCGTGCCTGAT R-CGAATTTCGGAGGGTTCTGC
	Mouse	F-CAGAGGAGAAGGCTGGTGTC R-CTGCCCCTTGGTGACATACT
	Human	F-CTGGGCAAGTCCAACAATTT R-CCAGCCCAGGATGTTGTAGT
MYH7	Rat	F-GCCTACAAGCGCCAGGCT R-CATCCTTAGGGTTGGGTAGCA
	Mouse	F-CTTCAACCACCACATGTTCG R-TCTCGATGAGGTCAATGCAG
	Human	F-GTGAAAGTGGGCAATGAGT R-TGGTGAAGTTGATGCAGAGC
Nppa/Anf	Rat	F-CGTATACAGTGCGGTGTCCAAC R-CCTCATCTTCTACCGGCATC
	Mouse	F-GTGCGGTGTCCAACACAGAT R-TTCCTCAGTCTGCTCACTCAGG
Nppb/Bnp	Rat	F-GGTCTCAAGACAGCGCCTTCC R-CTTCCTAAAACAACCTCAGCCCGTC
	Mouse	F-GCCAGTCTCCAGAGCAATTC R-GTTCTTTTGTGAGGCCTTGG
COL1A1	Mouse	F-GCCAAGAAGACATCCCTGAA R-GCCATTGTGGCAGATACAGA
Casp3	Mouse	F- GGGCCTGTTGAACTGAAAAA R- CCGTCCTTTGAATTTCTCCA
Casp9	Mouse	F- GCCAGAGGTTCTCAGACCAG R- AAGCCGTGACCATTTTCTTG
Bax	Mouse	F- t g c a g a g g a t g a t t g c t g a c R- g a t c a g c t c g g g c a c t t t a g
Bcl-2	Mouse	F- g g a c t t g a a g t g c c a t t g g t

		R- a g c c c c t c t g t g a c a g c t t a
ChIP-qPCR		
cFos promoter	Rat	F-CCTTGCGCTGCACCCTCAGA R-CGGCCGTGGAAACCTGCTGA
cJun promoter	Rat	F-TGTAGGAGCGCAGCGGAGCA R-CCCACCCGTCGCCATGGAGA
cFOS promoter	Human	F-TGTTATAAAAGCAGTGGCTGCG R-TCTTGGCTTCTCAGATGCTCG
cJUN promoter	Human	F-TCTCTCCGTCGCAACTTGTC R-ACGCAGCAGTTGCAAACATT
SMARCA4 promoter	Human	F-GGGAAGTTTTGCAGAGAAGGC R-CCTGGGAACCGCTTTGATCC